IOP PUBLISHING JOURNAL OF PHYSICS D: APPLIED PHYSICS

J. Phys. D: Appl. Phys. **42** (2009) 194013 (20pp) doi:10.1088/0022-3727/42/19/194013

REVIEW ARTICLE

Hybrid modelling of low temperature plasmas for fundamental investigations and equipment design

Mark J Kushner

Electrical Engineering and Computer Science Department, University of Michigan, 1301 Beal Ave., Ann Arbor, MI 48109-2122, USA

E-mail: mjkush@umich.edu

Received 12 May 2009, in final form 12 June 2009
Published 18 September 2009
Online at stacks.iop.org/JPhysD/42/194013

Abstract

The modelling of low temperature plasmas for fundamental investigations and equipment design is challenged by conflicting goals—having detailed, specialized algorithms which address sometimes subtle physical phenomena while also being flexible enough to address a wide range of process conditions. Hybrid modelling (HM) is a technique which provides many opportunities to address both fundamental physics and practical matters of equipment design. HM is a hierarchical approach in which modules addressing different physical processes on vastly disparate timescales are iteratively combined using time-slicing techniques. By compartmentalizing the physics in each module to accept given inputs and produce required outputs, different algorithms can be used to represent the same physical processes. In this manner, the algorithms best suited for the conditions of interest can be used without affecting other modules. In this paper, the basis and implementation of HM are discussed using examples from simulations of inductively coupled plasmas.

Abbreviations and symbols

$(\varepsilon, \vec{r}, \phi)$	dependence of energy, position and phase in harmonic period (or time)
$f(\varepsilon, \vec{r}, \phi)$	distribution function ($eV^{-3/2}$) in the gas phase or incident onto surfaces
$k_e(\vec{r}, \phi)$	electron impact rate coefficients ($cm^3\ s^{-1}$)
$S_e(\vec{r}, \phi)$	electron impact source functions ($cm^{-3}\ s^{-1}$)
$kS_e(\vec{r}, \phi)$	collectively, $k_e(\vec{r}, \phi)$ and $S_e(\vec{r}, \phi)$
$k(\vec{r}, \phi)$	heavy particle collisional rate coefficients ($cm^3\ s^{-1}$)
$S(\vec{r}, \phi)$	heavy particle collisional source functions ($cm^{-3}\ s^{-1}$)
$kS(\vec{r}, \phi)$	collectively, $k(\vec{r}, \phi)$ and $S(\vec{r}, \phi)$
$\vec{E}(\vec{r}, \phi)$, $\vec{B}(\vec{r}, \phi)$	electromagnetic fields ($V\ cm^{-1}$, G)
$\vec{E}\vec{B}(\vec{r}, \phi)$	collectively, $\vec{E}(\vec{r}, \phi)$ and $\vec{B}(\vec{r}, \phi)$
$\vec{E}_S(\vec{r}, \phi)$, $\vec{B}_S(\vec{r}, \phi)$	electro- and magnetostatic fields ($V\ cm^{-1}$, G)
$\vec{E}\vec{B}_S(\vec{r}, \phi)$	collectively, $\vec{E}_S(\vec{r}, \phi)$ and $\vec{B}_S(\vec{r}, \phi)$
$\Phi_S(\vec{r}, \phi)$	electrostatic potential (V)
$\Delta\Phi_b(t)$	electric potential across sheath as a jump boundary condition (V)
$\Phi\vec{E}_S(\vec{r}, \phi)$	collectively, $\Phi_S(\vec{r}, \phi)$ and $\vec{E}_S(\vec{r}, \phi)$
$\vec{M}_S(\vec{r}, \phi)$	magnetization (e.g. dipole moments) of materials external to plasma
$\upsilon(\vec{r}, \phi)$	electron collision frequency (s^{-1})
$\sigma(\vec{r}, \phi)$	conductivity ($1\ \Omega^{-1}\ cm^{-1}$)
$\rho(\vec{r}, \phi)$	charge density ($C\ cm^{-3}$)
$\rho_S(\vec{r}, \phi)$	charge density on surface (cm^{-3})
$\vec{j}(\vec{r}, \phi)$	current density ($A\ cm^{-2}$)
$\vec{j}_E(\vec{r}, \phi)$	external (or non-plasma) current density ($A\ cm^{-2}$)
$N(\vec{r})$	density (cm^{-3})

$\vec{\phi}(\vec{r})$	flux ($cm^{-2}\,s^{-1}$)
$\vec{\phi}_P(\nu,\vec{r})$	photon flux versus frequency ($cm^{-2}\,s^{-1}$)
ϕ	phase in harmonic cycle
$T(\vec{r})$	temperature (K or eV)
$N\phi T(\vec{r})$	collectively, $N(\vec{r})$, $\vec{\phi}(\vec{r})$ and $T(\vec{r})$
$\alpha(\vec{r})$	reaction probability on surfaces
$\beta_{ij}(\vec{r})$	probability of species i incident on surface producing species j
Δt_M,	time between calls to a module
CCP	capacitively coupled plasma
$\Delta H(\vec{r})$	change in enthalpy
DSMC	direct-simulation Monte Carlo
EEE	electron energy equation
EMCS	electron Monte Carlo simulation
FD	frequency domain
FDTD	finite difference, time domain
HM	hybrid modelling
HPEM	Hybrid Plasma Equipment Model
IEAD	ion energy and angular distribution
LFA	local field approximation
LTP	low temperature plasma
MERIE	magnetically enhanced reactive ion etching
SS, HSS	steady state, harmonic steady state
Td	E/N in Townsend ($1\,Td = 10^{-17}\,V\,cm^2$)

1. Introduction

Low temperature plasmas (LTPs) represent a particularly diverse discipline compared with other fields of plasma physics. The pressures over which LTP devices operate span nearly a factor of 10^9 (sub-millitorr to a few hundred atmospheres) [1]. There are many different excitation schemes, including inductively coupled plasmas (ICPs), capacitively coupled plasmas (CCPs) with single or multiple frequencies, electron cyclotron resonance (ECR), magnetically enhanced reactive ion etching (MERIE), dielectric barrier discharge (DBD) and magnetron, to name a few. The geometries of these devices range from simple cylindrical tubes to complex structures as found in plasma display panels. Excitation methods can be combined (for example, an ICP with a CCP bias on a substrate), be either continuous wave (cw) or pulsed; and the plasma can be in contact with a variety of materials which can substantially change its characteristics. Although the fundamentals of plasma transport are commonly investigated using gases having a minimum of chemistry in simple geometries, technological plasmas often use gas mixtures having complex chemistries that are influential in determining plasma properties, not to mention the intended use of those chemistries for material processing or photon generation.

The investigation of LTPs and the use of LTPs in technological devices have and will continue to benefit from computer modelling [2]. For example, plasma etching reactors are now designed in industry using multi-dimensional computer models [3, 4]. Impressive advances have been made in the development of computer models based on first principles, using particle-in-cell and fluid-hydrodynamic [5], to direct solutions of Boltzmann's equation [6]. These models have been used in both the investigation of fundamental physics and for the design of plasma equipment.

Having said that, the extreme diversity of LTPs places high expectations on computer modelling for equipment design. The model should address fundamental plasma phenomena so that *a priori* assumptions do not prejudice the result. At the same time, the model should be expansive enough to address a wide variety of plasma equipment using different excitation schemes and complex chemistries while being bounded by chemically active surfaces. From the perspective of investigating the fundamental physics, the best approach is perhaps using highly specialized models addressing a single type of excitation method in simple geometries for a limited variety of gases. From the perspective of technology development, a broader, more general capability is required. Ultimately, some compromise must be made.

In this paper, we describe one approach to first principles modelling of LTPs which is capable of addressing fundamental physics, while also attempting to address the more broad and general needs of designing plasma equipment. That technique is hybrid modelling. Hybrid models (HM) combine different modules which address different physical phenomena or modules that address the same phenomena using different computational algorithms which best match the operating conditions at hand. The flexibility of mixing-and-matching modules allows HM to address a wide range of physical and technological phenomena.

A particular implementation of HM, the Hybrid Plasma Equipment Model (HPEM), will be used as the basis for our discussion. Although the HPEM has been applied to a variety of reactor types (for example ECR [7], MERIE [8], magnetron [9], CCP [10] helicon [11], pulsed dc [12], ionized metal physical vapour deposition [13]), combinations of excitation schemes, real-time-control [14], three-dimensional transport [15] and dust particle transport [16], the discussion here will be restricted to two-dimensional (2D) ICP reactors with a CCP biased substrate.

In section 2 the fundamental bases of HM will be discussed followed by examples of modularity, timing and acceleration in section 3. The interchangeability of physics modules is discussed in section 4. Examples of different levels of complexity while including surface models is summarized in sections 5 and 6. Concluding remarks are in section 7.

2. Fundamentals of hybrid modelling

The basic premise of HM is combining computational modules which address different physical processes or address the same physical processes using different techniques. These modules transfer information between them in a hierarchical manner. As conditions (e.g. pressure), modes of excitation and perceived importance of processes change, modules can be exchanged, substituted or inserted to best address the parameters of interest. For example, in a HM hierarchy, if radiation transfer is deemed important, algorithms addressing these processes should be callable as an independently standing

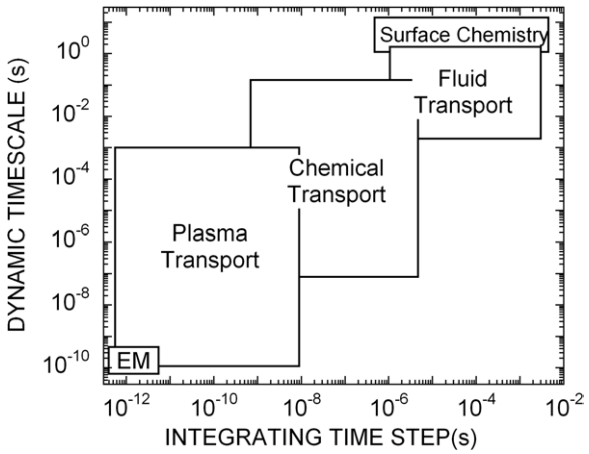

Figure 1. Schematic of the timescales required to be resolved in a comprehensive plasma equipment model. Dynamic timescale is the time for the phenomenon to come into equilibrium. The integration time step is the numerical resolution required in the algorithm.

module which receives data from and provides data to other modules without disturbing those modules' operation.

In the HM hierarchy, modules which address the same physics using algorithms should be totally transparent to other modules. For example, electromagnetics and plasma–wave interactions can be addressed by either a frequency domain (FD) or finite difference time domain (FDTD) method depending upon which is *best* for the plasma conditions. The operation of other modules which address plasma transport should not depend on which of these two methods is used provided the electromagnetics modules provide the necessary input.

In this context, *best* is a qualitative assessment. *Best* may not necessarily refer to the most intricate and detailed physical model for the particular phenomenon. Rather it refers to the most opportune description of the physics which is consistent with the end goal. For example, in using a 2D computer model to design a MERIE reactor in an industrial setting, cases must be physically accurate enough to guide the design but should not take an unreasonable amount of computer time so that many cases can be run. Achieving this goal might require some compromise on accuracy compared with a few executions of a model designed to illuminate a particular physical phenomenon.

It is on this issue that the needs of plasma equipment modelling and plasma physics modelling most diverge. To design industrial plasma equipment, an extraordinary dynamic range in time must be resolved, as shown in figure 1. In particular, two timescales must be resolved—the dynamic timescale required for a phenomenon to come to a steady state (SS) and the integrating time step required to numerically resolve the phenomenon in a stable manner. The dynamic range of these timescales could be as large as 10^{12}, from ps for the integrating time step in a FDTD simulation to seconds for surface chemistry to come to a SS. When considering the additional computational load for multi-dimensional simulations of multi-scale problems (e.g. tens of micrometres for sheaths to a metre for the reactor), it becomes clear that direct integration of coupled sets of differential equations addressing all of the phenomena (or a particle based equivalent approach) will be extremely challenging.

HM is a hierarchical approach to modelling whose goals include integration of diverse, first principles physics modules which can be implemented over a large enough dynamic range in time to be relevant to equipment modelling. HM has the following formulaic approach.

- Compartmentalize physical processes into relatively independent modules.
- Establish hierarchical relationships between the modules (information flow between modules).
- Determine the relative timescales for integration within a module to resolve the physics and the time for exchange of information between modules.

Since it is difficult to speak totally in the abstract about HM, reference will be made to one particular implementation of HM. That implementation, HPEM, has been developed using HM principles to address as fundamental physics as possible while retaining the flexibility of a general plasma equipment model capable of technology development. The major modules contained in the HPEM are listed in table 1 with their required input data and their output products.

Although the HPEM is capable of addressing harmonic through pulsed dc applications, many of the applications of interest in, for example, materials processing use harmonically applied electric fields. As such, we will refer to time variant quantities according to their phase in a harmonic cycle, ϕ. The reader should, however, interpret the notation as more generally referring to time dependence, whether harmonic or not.

In an LTP virtually all physical parameters are either directly or indirectly dependent on virtually all other physical parameters. For example, the solution of Maxwell's equations describing the penetration of an electromagnetic wave into a plasma depends on the spatial distribution of conductivity (in the absence of anomalous effects). Conductivity is a function of charged particle densities and collision frequency. Electron density and collision frequency are functions of the electron energy distributions, $f(\varepsilon, \vec{r}, \phi)$, which are in turn dependent on the time history of the electric field, gas density and mole fractions, including excited states.

Clearly, self-consistently modelling the penetration of an electromagnetic wave into a low pressure plasma in, for example, an ICP reactor is a complex undertaking. However, in spite of this complexity it is possible to create a computational module that solves Maxwell's equations while having specific inputs and outputs. To solve Maxwell's equations in the electromagnetics module (EMM) of the HPEM, one requires as inputs coil currents, materials properties surrounding the plasma (e.g. permittivity, permeability, conductivity) and plasma conductivity, $\sigma(\vec{r}, \phi)$ as a function of position and possibly phase. (Although the EMM has the capability of addressing electrostatics with a non-zero charge density, $\rho(\vec{r}, \phi)$, we will restrict discussion here to the purely electromagnetic case.)

The outputs of the EMM are the spatially dependent vector components and phases of electric and magnetic fields,

Table 1. Major modules in the HPEM.

		Inputs	Outputs	References
ASM	Analyltic sheath module	$N\phi T(\vec{r})$, $\vec{B}_S(\vec{r},\phi)$	$\Delta\Phi_b(t)$	[17]
MSM	Magnetostatic module	$\vec{j}_E(\vec{r},\phi)$, $\vec{M}_S(\vec{r},\phi)$	$\vec{B}_S(\vec{r},\phi)$	[18]
EMM	Electromagnetics module	$\vec{B}_S(\vec{r},\phi)$, $\sigma(\vec{r},\phi)$, $\vec{j}(\vec{r},\phi)$, $\vec{j}_E(\vec{r},\phi)$	$\vec{E}\vec{B}(\vec{r},\phi)$	[11]
EETM	Electron energy transport module	$N(\vec{r})$, $\vec{E}\vec{B}_S(\vec{r},\phi)$, $\vec{E}\vec{B}(\vec{r},\phi)$	$f(\varepsilon,\vec{r},\phi)$, $kS_e(\vec{r},\phi)$	[19]
FKPM	Fluid kinetics-poisson module	$\vec{E}\vec{B}(\vec{r},\phi)$, $\vec{B}_S(\vec{r},\phi)$, $kS_e(\vec{r},\phi)$, $\alpha_S(\vec{r})$, $\beta_S(\vec{r})$	$N\phi T(\vec{r})$, $\Phi\vec{E}_S(\vec{r},\phi)$	[19]
SKM	Surface kinetics module	$f(\varepsilon,\vec{r},\phi)$, $\vec{\phi}(\vec{r})$	$\alpha(\vec{r})$, $\beta_{ij}(\vec{r})$	[20]
DTM	Dust transport module	$\vec{E}\vec{B}(\vec{r},\phi)$, $\vec{B}_S(\vec{r},\phi)$, $\Phi\vec{E}_S(\vec{r},\phi)$, $N\phi T(\vec{r})$	Dust particle positions and trajectories	[16]
RTMCM	Radiation transport Monte Carlo module	$N\phi T(\vec{r})kS_e(\vec{r},\phi)$, $kS(\vec{r},\phi)$	$\vec{\phi}_P(\nu,\vec{r})$	[21]
PCMPM	Plasma chemistry Monte Carlo module	$N\phi T(\vec{r})kS_e(\vec{r},\phi)$, $kS(\vec{r},\phi)$	$\vec{\phi}(\vec{r})$	[13]
RTCM	Real time control module	Sensor readings of plasma and circuit parameters	Changes in actuator settings	[14]
SM	Sputter module	$N\phi T(\vec{r})kS_e(\vec{r},\phi)$, $kS(\vec{r},\phi)$	$\vec{\phi}(\vec{r})$, $\Delta H(\vec{r})$	[13, 18]
IMCS	Ion Monte Carlo simulation	$N\phi T(\vec{r})kS_e(\vec{r},\phi)$, $kS(\vec{r},\phi)$	$f(\varepsilon,\vec{r},\phi)_{ION}$	[9]
CM	Circuit module	$\vec{j}(\vec{r},\phi)$	Voltages on electrodes	[22]

$\vec{E}(\vec{r},\phi)$ and $\vec{B}(\vec{r},\phi)$, collectively referred to as $\vec{E}\vec{B}(\vec{r},\phi)$ To a large degree, the solution of Maxell's equations in the EMM does not depend upon how $\sigma(\vec{r},\phi)$ and other input quantities were obtained—the EMM merely requires these quantities to perform its duties.

In the same modular fashion, there are physical processes that use $\vec{E}\vec{B}(\vec{r},\phi)$ as input to produce other quantities. Boltzmann's equation or its moments are solved in the electron energy transport module (EETM) of the HPEM to produce $f(\varepsilon,\vec{r},\phi)$. Solving for $f(\varepsilon,\vec{r},\phi)$ can be performed using the electron Monte Carlo simulation (EMCS) which requires $\vec{E}\vec{B}(\vec{r},\phi)$ as input. The EETM produces electron impact rate coefficients $k_e(\vec{r},\phi)$ and sources $S_e(\vec{r},\phi)$, collectively referred to as $kS_e(\vec{r},\phi)$, as output as a function of position and phase which are derived from $f(\varepsilon,\vec{r},\phi)$. To a large degree, solving Boltzmann's equation in the EMCS for $f(\varepsilon,\vec{r},\phi)$ does not depend upon how the $\vec{E}\vec{B}(\vec{r},\phi)$ were produced—it merely requires these quantities. And because the EETM does not depend on how the $\vec{E}\vec{B}(\vec{r},\phi)$ were produced, any method appropriate for the conditions at hand can be used in the EMM to produce these quantities. For example, the EMM could use either a FD or FDTD method to produce $\vec{E}\vec{B}(\vec{r},\phi)$, and the method of solution of Boltzmann's equation in the EETM would not be affected.

As a side note, the interchange of physical data between modules is well illustrated by the EMM and EMCS. The EMM requires a relationship between $\sigma(\vec{r},\phi)$ and $\vec{E}\vec{B}(\vec{r},\phi)$ to produce plasma current densities $\vec{j}(\vec{r},\phi)$—that is $\vec{j}(\vec{r},\phi) = F(\sigma, E, B)$. For electron transport that is local and collisional, $\vec{j}(\vec{r},\phi) = \sigma(\vec{r})\vec{E}(\vec{r},\phi)$. However, for non-local conditions, the EMCS can provide $\vec{j}(\vec{r},\phi)$ as a phase derived integral of electron trajectories which contains a past history of electron acceleration by $\vec{E}\vec{B}(\vec{r},\phi)$. The solution of Maxwell's equation in the EMM does not depend on where $\vec{j}(\vec{r},\phi)$ comes from, it merely requires $\vec{j}(\vec{r},\phi)$. A properly structured solution of Maxwell's equation in a HM should seamlessly accept $\vec{j}(\vec{r},\phi)$ as being simply $\sigma(\vec{r})\vec{E}(\vec{r},\phi)$ or as being derived from the EMCS. This seamless acceptance enables the HM to address both local and non-local conditions without perturbing the rest of the HM.

In a similar vein, if the role of the EETM is to accept $\vec{E}\vec{B}(\vec{r},\phi)$, electrostatic fields $\vec{E}_S(\vec{r},\phi)$ and magnetostatic fields $\vec{B}_S(\vec{r},\phi)$ (collectively referred to as $\vec{E}\vec{B}_S(\vec{r},\phi)$) to produce $kS_e(\vec{r},\phi)$, many different techniques can be used to process the inputs and generate the outputs. For example, if the conditions are high pressure with slowly varying electric fields having nominal gradients, a local field approximation (LFA) may be appropriate. If the conditions include time varying fields with non-local transport, the EMCS may be more appropriate. If $f(\varepsilon,\vec{r},\phi)$ is composed dominantly of a single group, then an electron energy equation (EEE) might be the best approach. If $f(\varepsilon,\vec{r},\phi)$ contains a beam component resulting from secondary electron emission, then a combined beam (EMCS)–bulk (EEE) technique might be best. Again, the modules which use $kS_e(\vec{r},\phi)$ will not be affected by the choice of which technique is used in the EETM to process the inputs and generate the outputs other than the accuracy of the chosen method.

The fluid kinetics-Poisson module (FKPM) of the HPEM is where the densities, momenta and temperatures of neutral and charged species are produced. Due to the tight coupling of electrostatic fields to the densities of charged particles, the solution of Poisson's equation for the electrostatic potential, $\Phi_S(\vec{r},\phi)$, is performed within the FKPM. The FKPM accepts as inputs $kS_e(\vec{r},\phi)$, $\vec{E}\vec{B}(\vec{r},\phi)$ and $\vec{B}_S(\vec{r},\phi)$. It produces as output the densities $N(\vec{r})$, fluxes $\vec{\phi}(\vec{r})$ and temperatures

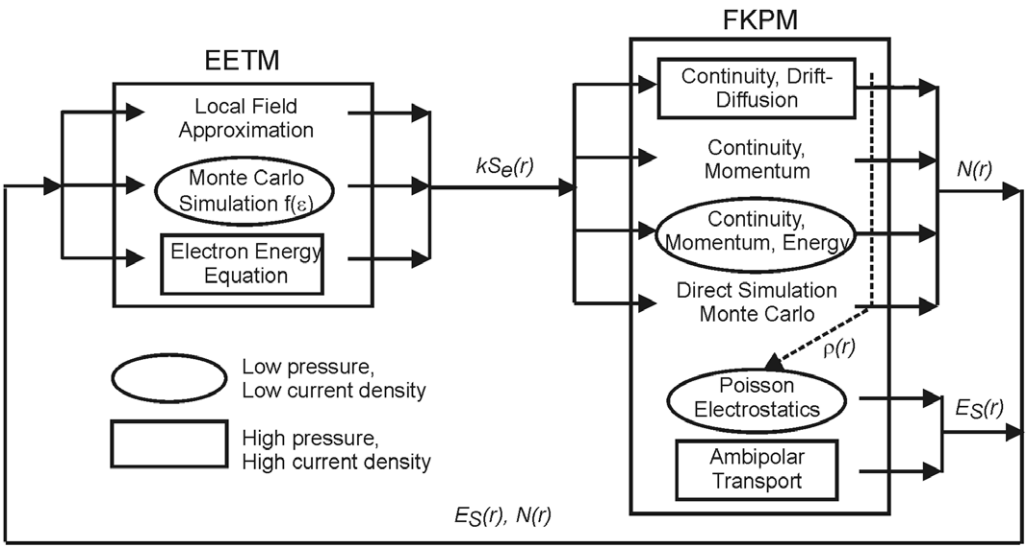

Figure 2. Paths through the EETM and FKPM for a case operating at low pressure with low current density; and a case operating at high pressure with high current density.

$T(\vec{r})$ (collectively abbreviated as $N\phi T(\vec{r})$), of neutral and charged species; and $\Phi_S(\vec{r},\phi)$ which provides $\vec{E}_S(\vec{r},\phi)$. The FKPM also produces rate coefficients and source functions $k(\vec{r},\phi)$and $S(\vec{r},\phi)$ for heavy particle reactions, collectively referred to as $kS(\vec{r},\phi)$.

Again, there are many techniques that can be used to produce $N\phi T(\vec{r})$ depending on the conditions at hand. At low pressures, one might use the full hydrodynamic conservation equations (continuity, momentum and energy) or use a direct-simulation Monte Carlo (DSMC) technique. At high pressures, a continuity equation using drift-diffusion approximation might suffice. Similarly, $\Phi_S(\vec{r},\phi)$ can be obtained by a direct solution of Poisson's equation or from an ambipolar approximation.

The EMM and EETM use the outputs of the FKPM to perform their functions. The ability of the EMM and EETM to perform their functions does not depend on the method used to produce $N\phi T(\vec{r})$ and $\vec{E}_S(\vec{r},\phi)$, other than in the accuracy of the chosen method, they merely require those quantities.

Consider a simple dc positive column discharge which requires only the EETM to produce $kS_e(\vec{r},\phi)$, and the FKPM to produce $N\phi T(\vec{r})$ and $\vec{E}_S(\vec{r},\phi)$. A schematic of the HPEM that captures those modules is in figure 2. The path through the modules for a high pressure, high current density case might begin by using an EEE in the EETM to produce $kS_e(\vec{r},\phi)$. The path would continue in the FKPM, where a continuity equation with drift-diffusion fluxes is used to produce $N\phi T(\vec{r})$ and an ambipolar approximation is used to produce $\vec{E}_S(\vec{r},\phi)$. For a low pressure, low current density conditions, these options might instead include the EMCS in the EETM. In the FKPM, the options might include continuity, momentum and energy equations and Poisson's equation.

3. Modules, timing and accelerating

In this section, interchangeable modules, their sequencing, timing and acceleration in the HM hierarchy will be described.

3.1. Continuity, momentum, energy and Poisson's equation

Once the physical processes of interest are modularized, one can then choose a model to represent those processes which is *best* for the conditions at hand. As an example, some of the options available in the FKPM of the HPEM will be discussed for transport of charged and neutral particles. In all options, the continuity equation is solved,

$$\frac{\partial N_i}{\partial t} = -\nabla\cdot\vec{\phi}_i + S_i, \tag{1}$$

where N_i, $\vec{\phi}_i$ and S_i are the species density, flux and source for species i. Various options can then be used to produce $\vec{\phi}_i$

Option 1A. Drift diffusion without B-field:

$$\vec{\phi}_i = -D_i\nabla N_i + q_i\mu_i N_i\vec{E}, \tag{2}$$

where D_i, q_i and μ_i are the diffusion coefficient, charge and mobility of species i.

Option 1B. Drift diffusion with B-field:

$$\vec{\phi}_i = \bar{\bar{\mu}}_i\cdot\left(q_i N_i\vec{E}_S - \frac{kT_i}{|q_i|}\nabla N_i\right), \tag{3}$$

where the mobility is a tensor quantity and T_i is the temperature.

Option 1C. Drift diffusion using Schaffeter–Gummel fluxes [23] which is essentially an auto-selecting upwind differentiation technique. In principle, this option is a numerical implementation of option 1A. In practice, when using the Schaffeter–Gummel formulation, the dependence of the flux on electric field is non-linear whereas in option 1A the dependence is linear. Therefore, the Jacobian elements in implicit implementations must be linearized or numerically derived.

Option 2. Momentum equation:

$$\frac{\partial \vec{\phi}_i}{\partial t} = -\frac{1}{m_i}\nabla(N_i k T_i) - \nabla\cdot(N_i \bar{v}_i \bar{v}_i) + \frac{q_i}{m_i} N_i(\bar{E}_S + \bar{v}_i \times \bar{B}) - \nabla\cdot\bar{\bar{\nu}}_i - \sum_j \frac{m_j}{m_i + m_j} N_i N_j (\bar{v}_i - \bar{v}_j)\nu_{ij}, \quad (4)$$

where $\bar{v}_i$ is velocity, $\bar{\bar{\nu}}_i$ is the viscosity tensor (used only for neutral species) and ν_{ij} is the collision frequency between species i and species j.

Option 3. Momentum equation plus an energy equation:

$$\frac{\partial(N_i c_i T_i)}{\partial t} = \nabla\cdot\kappa\nabla T_i - P_i\nabla\cdot\vec{v}_i - \nabla\cdot(N_i\vec{v}_i\varepsilon_i) + \frac{N_i q_i^2 \nu_i}{m_i(\nu_i^2+\omega^2)}E_\Theta^2 + \frac{N_i q_i^2}{m_i\nu_i}E_S^2 + \sum_j 3\frac{m_{ij}}{m_i+m_j}N_i N_j \nu_{ij} k_B(T_j - T_i) \pm \sum_j 3N_i N_j R_{ij} k_B T_j, \quad (5)$$

where c_i is the heat capacity, κ_i is the thermal conductivity, P_i is the partial pressure and k_{ij} is the rate coefficient for formation of the species by collisions between heavy particles. There are heating contributions for charged particles from both the electrostatic and electromagnetic fields. In this particular example, we show a contribution from heating in the azimuthal direction by an inductively coupled electric field.

Due to the tight coupling between densities and the electric potential, solution of Poisson's equation, or its ambipolar equivalent, is performed in the FKPM. Again, there are several options that can be chosen for the conditions at hand.

Option 1. Explicit Poisson's equation:

$$-\nabla\cdot\varepsilon\nabla\Phi_S(t) = \sum_i q_i N_i(t) + \rho_S(t), \quad (6)$$

where $\rho_S(t)$ is the charge density in or on non-plasma materials.

$$\frac{d\rho_S(t)}{dt} = -\nabla\cdot\left(\sum_i q_i\phi_{Si} - \sigma_M\nabla\Phi_S\right), \quad (7)$$

where the first term is sum of the fluxes of charged species incident onto surfaces in contact with the plasma, ϕ_{Si}, and the second term is the current density within materials having conductivity σ_M. In practice, option 1 is rarely used due to the limitation on the time step presented by the dielectric relaxation time, $\Delta t = \varepsilon_0/\sigma$, which can be as small as a few picoseconds.

Option 2. Semi-implicit Poisson's equation:

$$-\nabla\cdot\varepsilon\nabla\Phi_S(t+\Delta t) = \sum_i q_i(N_i(t) - \Delta t\nabla\cdot\phi_i(\Phi_S(t+\Delta t)) + S_i(t)) + \rho_S(t) - \Delta t\nabla\cdot\begin{pmatrix}\sum_i q_i\phi_{Si}(\Phi_S(t+\Delta t))\\ -\sigma_M\nabla\Phi_S(t+\Delta t)\end{pmatrix}. \quad (8)$$

Using this option, the potential is solved for at a future time. Charge densities are provided by their present values plus an incremental prediction of their values at the future time based on the divergence of their fluxes provided by drift-diffusion expressions. The appearance of the potential in the drift-diffusion fluxes provides a degree of implicitness.

Option 3. Semi-implicit Poisson with implicit electrons and predictor–corrector ions. This option is otherwise the same as option 2 except that the electron density is implicitly solved for simultaneously with Poisson's equation.

$$-\nabla\cdot\varepsilon\nabla\Phi_S(t+\Delta t) = q_e n_e(t+\Delta t) + \cdots \quad (9a)$$

$$n_e(t+\Delta t) = n_e(t) - \nabla\cdot\vec{\phi}_e(\Phi_S(t+\Delta t)) + S_e(t). \quad (9b)$$

With $\vec{\phi}_e$ given by the drift-diffusion techniques, the equations can be implicitly solved by appearance of the potential in the electron continuity equation.

Option 4. Semi-implicit Poisson with implicit electron densities and fluxes. The expression for Φ_S is the same as for option 3.

$$n_e(t+\Delta t) = n(t) - \nabla\cdot\vec{\phi}_e(t+\Delta t) + S_e(t), \quad (10)$$

$$\vec{\phi}_e(t+\Delta t) = \vec{\phi}_e(t) - \Delta t\left(\frac{1}{m_e}\nabla(n_e k T_{ei}) - \nabla\cdot(N_e\bar{v}_e\bar{v}_e) + \frac{q_e}{m_e}n_e(\bar{E}_S + \bar{v}_e\times\bar{B}) - \sum_j\frac{m_e}{m_i+m_j}n_e N_j(\bar{v}_e - \bar{v}_j)\nu_{ej}\right). \quad (11)$$

Option 5. Semi-implicit ambipolar approximation. In this option, Φ_S is obtained by simultaneously requiring current continuity and charge neutrality.

$$-\nabla\cdot j(N_i(t), \Phi_S(t+\Delta t)) = \sum_i q_i S_i(t), \quad (12)$$

$$n_e(t) = \sum_{\text{ions}} q_i N_i(t). \quad (13)$$

Option 6. Any other option including a sheath model. In this option, a sheath potential is computed at the boundary of the plasma where the thickness of the sheath is not resolved by the numerical mesh used to solve Poisson's equation. Under these conditions, a potential jump across the sheath at the boundary of plasma, $\Delta\Phi_b(t)$, is added to the solution of Poisson's equation. For example,

$$-\nabla\cdot\varepsilon\nabla(\Phi_S(t) + \Delta\Phi_b(t)) = \sum_i q_i N_i(t) + \rho_S(t). \quad (14)$$

$\Delta\Phi_b(t)$ is obtained by the analytic sheath module (ASM).

In all options for solving Poisson's equation, ion fluxes can optionally be derived from solving their momentum equations as opposed to using a drift-diffusion formulation. In these cases, the direct semi-implicit solution for the ion fluxes with Φ_S is lost. This results from the fluxes that determine future ion densities not being linear functions of electric potential, as would occur when using drift-diffusion fluxes. When using ion

momentum equations, $\vec{\phi}_{\rm ion}(t+\Delta t)$ is not an easily quantified function of Φ_S and so even numerically constructing Jacobian elements is difficult.

In principle, the ion momentum equations could be included in the matrix for semi-implicit solutions for electron and ion densities and Φ_S. In practice, this becomes computationally burdensome when there are many ion species. We have found, however, that even an approximate prediction for the ion densities at future times, $N(t+\Delta t)$, provides additional stability and the ability to take larger time steps. This prediction can be constructed by recording a short past history of fluxes and source functions, and numerically deriving derivatives. For example,

$$N(t+\Delta t) = N(t) + \Delta t \begin{pmatrix} -\nabla\cdot\left(\phi(t) + \Delta t \dfrac{{\rm d}\phi(t)}{{\rm d}t}\right) \\ +S(t) + \Delta t \dfrac{{\rm d}S(t)}{{\rm d}t} \end{pmatrix}, \tag{15}$$

where ${\rm d}\phi(t)/{\rm d}t$ and ${\rm d}S(t)/{\rm d}t$ are derived from a past history of fluxes and source functions.

The HM hierarchy extends to the method used to solve the matrices obtained from implementing these options. For example, when using finite differences for discretization on a structured mesh, the numerical molecule contains contributions only from nearest neighbours in the absence of magnetostatic fields. That is, it is a five-point numerical molecule. Each of the nearest neighbour points are connected to the centre point by a coefficient containing transport coefficients and geometrical information. In this case, an iterative method such as successive-over-relaxation (SOR) is a fast and efficient means of solving the matrix containing Poisson's equation. When using a static magnetic field, the numerical molecule has nine points and contains next-nearest neighbours which do not share a coefficient with the centre point. For these conditions, an iterative or direct sparse matrix technique is preferred. In the HM, construction of the matrices to implement these options should be independent of the solution method.

The choice for which method for constructing fluxes, solving Poisson's equation and deriving transport coefficients is based, in principle, on computing resources. If computing resources were not limited, the most detailed and highest order formulation would provide the most accurate result regardless of the operating conditions. In practice, computing resources are limited. So including the minimum level of sophistication required to obtain the desired accuracy determines which method is chosen. (See discussion accompanying figure 2.)

3.2. Time dependences

The advantage of using a non-modular approach to plasma modelling is that, in principle, all processes can be simultaneously integrated in time as a large set of partial-differential equations. This provides unambiguous time dependence. A weakness to the HM approach is that modules are typically executed in sequence. Equations may be directly integrated in time within a given module which explicitly resolves the harmonic periods or other transients. However during these integrations, quantities received from other modules are either time-invariant, interpolated from fixed time dependences or Fourier analysed to provide harmonic quantities. In either case, there is no lock-step consistency of time dependent quantities except after having achieved a true SS or HSS.

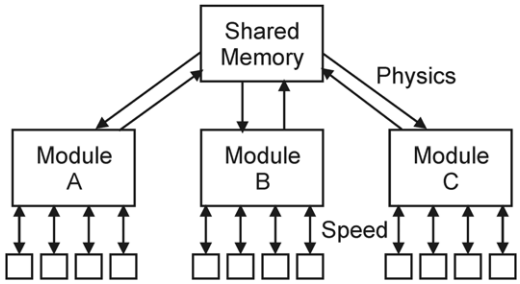

Figure 3. Schematic of a parallel computational technique that enables real-time resolution of long term transients. Modules are executed on different processors, exchanging information with other modules through shared memory (or message passing). This is performed to optimize the physical representation and will not necessarily greatly improve the speed of computation. Finer grain parallelization within a module can be implemented to speed the calculation.

For example, electron impact source functions from the EETM, $S_e(\vec{r},\phi)$, may be provided to the FKPM as a function of phase during a harmonic cycle. Within the FKPM, $S_e(\vec{r},\phi)$ is interpolated to give time dependent values. However, the values of $S_e(\vec{r},\phi)$ at any given position or phase are not updated until the next execution of the EETM. Ultimately, the resolution with which a HM can address long term transients is determined by the interval time for exchanging information between the modules. In the HPEM, one cycle through the modules with each module sequentially accepting data from the previous module and providing data for the next is called an iteration.

An exception to the sequential nature of HM is the use of parallel processing. In principle, each module of the HPEM could be executed on a separate processor of a parallel computer (and have further, fine grain parallelization within a module), as shown in figure 3. Proof of principle of this concept can be found in [24]. In this manner, data can be exchanged between the modules on a real time basis and long term transients can be resolved with arbitrary accuracy.

In practice, a HM must resolve not only the harmonic behaviour within an rf cycle but also long term time evolution of plasma properties occurring over what may be millions of cycles. That is, HM must address extreme ranges in dynamic and integrating time steps. In the HPEM, this is achieved using time-slicing techniques. In time slicing, a given module is executed while the input values from other modules are held constant or allowed to vary in time in a predetermined way. The time spent in any given module is determined by its dynamic timescale.

For example, consider an electron swarm in a high pressure gas (greater than many torr) where values of E/N are greater than many Td. Under these conditions, $f(\varepsilon,\vec{r},\phi)$ of the electron swarm will come into equilibrium with the current

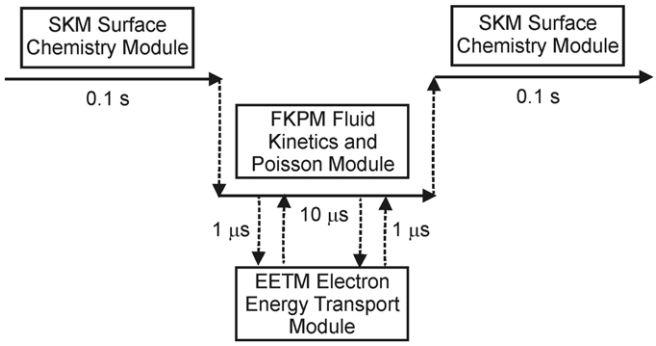

Figure 4. Schematic of time slicing between modules where the final outcome is a SS solution. Sub-time slicing may occur between the FKPM and EETM as those modules are more tightly coupled.

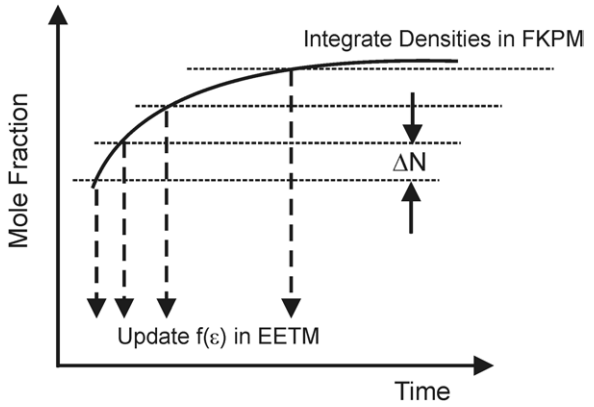

Figure 5. Schematic of time-slicing sequence wherein $f(\varepsilon)$ in the EETM is updated after mole fractions of gas phase species in the FKPM change by a specified amount. This technique works well for time integration to a SS or HSS.

values of gas densities and mole fractions in only a few to tens of nanoseconds. This timescale is typically short compared with the time over which those gas densities and mole fractions will change. One can therefore hold the values of $k_e(\vec{r},\phi)$ derived from $f(\varepsilon,\vec{r},\phi)$ constant while the rate equations for the plasma and gas densities are integrated. That integration can proceed until those densities change significantly enough to affect $f(\varepsilon,\vec{r},\phi)$. At that time, $f(\varepsilon,\vec{r},\phi)$ would need to be updated.

An example of a time-slicing scheme is shown in figure 4 for interaction between the surface kinetics module (SKM), the FKPM and the EETM. The dynamic timescale of the SKM is 0.1 s; for the FKPM is 10 μs and of the EETM is 1 μs. So in time slicing, the SKM is executed for some fraction of 0.1 s while holding fluxes to the surface from the FKPM constant. The FKPM is executed for some fraction of 10 μs holding surface reaction probabilities from the SKM and rate coefficients from the EETM constant. Since the FKPM and EETM are fairly tightly coupled there could be sub-time slicing between those modules, where the EETM is executed for some fraction of 1 μs, prior to updating fluxes to surfaces for the next iteration of the SKM.

To implement time slicing one needs some fore-knowledge of the degree of change in quantities in another module that affect the results of the current module. For example, in time slicing between the FKPM and EETM, one needs some knowledge of the changes in mole fractions, pressures or E/N that will produce a significant change in $f(\varepsilon,\vec{r},\phi)$, that would in turn affect rate and transport coefficients. When these changes in densities or E/N exceed a given limit, $f(\varepsilon,\vec{r},\phi)$ would need be updated. These changes can be automatically sensed within the model or externally specified.

For example, consider modelling a SS dc discharge using the EETM and FKPM. The SS is achieved by time integrating the continuity equations coincident with solution of Poisson's equation. An EMCS is used to compute $f(\varepsilon,\vec{r},\phi)$ which produce $Sk_e(\vec{r},\phi)$ used in the continuity equations in the FKPM. For this example, assume that the electron swarm in the EMCS equilibrates with $N\phi T(\vec{r})$ and $\vec{E}_S(\vec{r},\phi)$ provided by the FKPM in tens of nanoseconds whereas the densities in the FKPM significantly change on millisecond timescales. Furthermore, a change in mole fractions or E/N of a few per cent is considered sufficient to trigger a re-computation of $f(\varepsilon,\vec{r},\phi)$.

For these conditions, time slicing between modules is schematically shown in figure 5. The sequence might consist of an initial call to the EETM to provide starting values of $Sk_e(\vec{r},\phi)$. The densities are time integrated in the FKPM for a few milliseconds or until the change in mole fractions or E/N exceeds a threshold value. At that time, the new densities and E/N are transferred back to the EETM to update the $Sk_e(\vec{r},\phi)$. As the time integration approaches the SS, the frequency with which the EETM is called decreases.

A strength of HM is in addressing SS or harmonic steady-state (HSS) solutions. For these conditions, the timing between calls to modules is not particularly important as long as the solution eventually converges to SS or HSS values. (To resolve a true transient, the time between calls to a module, Δt_M, should not be greater than the time you wish to resolve during the transient.) Although it is critical that within, for example, the EETM and the FKPM that a harmonic cycle be explicitly resolved in the solution of Poisson's or Boltzmann's equations, it is not necessary to resolve the harmonic cycles over very long times if time slicing is used.

The HSS provides many opportunities to speed solutions. For example, consider the EMCS within the EETM in which the trajectory of electron pseudoparticles are tracked as a function of time to produce $f(\varepsilon,\vec{r},\phi)$. The electrostatic fields and densities computed in the FKPM as a function of phase $[E_S(\vec{r},\phi),N(\vec{r},\phi)]$, electromagnetic fields computed in the EMM $[\vec{E}\vec{B}(\vec{r},\phi)]$ and magnetostatic fields computed in the MSM $[\vec{B}_S(\vec{r})]$ are used in the EMCS to advance the trajectories of the pseudoparticles. These values are transferred to the EETM as a lookup table or as Fourier analysed harmonic components that provide their values as a function of position and phase. As the electrons advance in the phase of the harmonic cycle, $E_S(\vec{r},\phi)$ and $\vec{E}\vec{B}(\vec{r},\phi)$are interpolated from their values recorded in other modules. The electron energies (and in some cases their vector velocity components) are recorded and binned according to the instantaneous phase to produce $f(\varepsilon,\vec{r},\phi)$. As many tens

to hundreds of rf cycles may be computed in any given call to the EETM, statistics are improved by binning the energies of the pseudoparticles by their phase in the harmonic cycle. The resulting $f(\varepsilon, \vec{r}, \phi)$ are then used to produce tabular (or Fourier analysed) values of $Sk_e(\vec{r}, \phi)$ that are used in other modules.

Using time-slicing techniques, the values of $Sk_e(\vec{r}, \phi)$ provided by the EETM can be used for times far in excess of the integration time in the EETM provided the change in densities and fields in other modules have not exceeded threshold values.

3.3. Surface chemistry

Surface chemistry, even in simple rare gas mixtures, is important in providing boundary conditions for species intersecting with and returning from surfaces in contact with the plasma. Surface chemistry can be straightforwardly included in a HM provided the boundary conditions for plasma species are formulated in a hierarchical manner. In the HPEM, this is accomplished using the surface kinetics model (SKM).

In the FKPM, the boundary conditions for gas phase species incident onto surfaces and returning from surfaces are addressed using a 'flux-in/flux-out' methodology. Using this technique, densities of gas phase species on surfaces are not explicitly specified in the FKPM. Rather the disposition of fluxes incident on the surface is specified as either *disappearing* (that is, the flux is consumed by striking the surface) or generating *returning species* (that is, fluxes of other species are emitted by the surface by virtue of the incident flux.) In HM hierarchical manner, these interactions are captured in surface reaction probabilities which, from the perspective of the FKPM, are provided by other modules. The execution of the FKPM does not depend on how the coefficients were produced, it merely requires them.

For example, consider gas phase species N_k, at a mesh point adjacent to surface material m. The time rate of change of N_k resulting from surface processes in the FKPM is given by

$$\frac{dN_k}{dt} = \eta\left(-\phi_k \sum_{n,j} S_{jm}\kappa_{kjn} + \sum_{n,j} \phi_n S_{jm}\kappa_{njk}\right)$$
$$= \eta\left(-\phi_k \beta_{km} + \sum_j \phi_j \chi_{jmk}\right), \tag{16}$$

$$\beta_{km} = \sum_{n,j} S_{jm}\kappa_{kjn}, \qquad \chi_{jmk} = \sum_j S_{jm}\kappa_{njk},$$

where ϕ_k is the flux of species k, S_{jm} is the coverage of surface species j on material m, and κ_{njk} is the probability of reaction of gas phase species n striking surface species j producing gas phase species k. η is the factor accounting for the numerical discretization of the divergence term between the gas phase mesh point and the surface point. β_{km} is the total reaction probability of species k on material m and χ_{jmk} is the probability of gas species j incident on material m producing gas species k. The first term in equation (16) accounts for the *disappearance* of ϕ_k striking the surface by virtue of surface reactions. The second term accounts for the *generation* of ϕ_k being emitted from the surface due to fluxes of other species, including photons, incident onto the surface. (Note that the ϕ_k onto the surface has both a random thermal component and a directed convective component.)

In the HM hierarchy, the role of the SKM is to compute the values of S_{jm} and so the values β_{km} and χ_{jmk} for use in the FKPM. Using time-slicing techniques, the SKM is periodically called to update the values β_{km} and χ_{jmk} without interfering with the FKPM. Within the SKM, any technique that accepts ϕ_k, and produces β_{km} and χ_{jmk} is compatible with the FKPM.

In the HPEM, a multi-layer, surface site balance model is used to provide β_{km} and χ_{jmk}. Briefly, the SKM integrates a set of rate equations for (a) the fractional coverages of surface species, (b) the thickness and composition of layers overlying base surface sites and (c) fractional coverage of adsorbed species on the surface in direct contact with the plasma. These coverages are computed at every mesh point of materials in contact with the plasma. For example,

$$\frac{dS_{jk}}{dt} = -S_{jk}\left(\sum_{n,m} \phi_{nk}\lambda_{njm}\theta_k\zeta_k + \sum_{n,m} S_{nk}\xi_{jnm}\right)$$
$$+ \sum_{n,m} \phi_{nk}S_{mk}\lambda_{nmj}\theta_k\zeta_k + \sum_{nm} S_{mk}S_{nk}\xi_{nmj}, \tag{17}$$

$$\lambda_{njm} = \int f_{nk}(\varepsilon)\, p_{njm}(\varepsilon) d\varepsilon, \tag{18}$$

$$p_{njm}(\varepsilon) = \begin{pmatrix} p_0 \dfrac{\varepsilon^b - \varepsilon_t^b}{\varepsilon_0^b - \varepsilon_t^b} \\ p_0 \,\mathrm{Max}(1 - \varepsilon/\varepsilon_M) \end{pmatrix}, \tag{19}$$

where for surface location k, S_{jk} is the fractional surface coverage of species j, ϕ_{nk} is the flux of gas phase species or photon n, λ_{njm} is the probability of reaction of gas phase species n with surface species j producing surface species m, ξ_{njm} is the probability of reaction of surface species phase n with surface species j producing surface species m and $f_{nk}(\varepsilon)$ is the energy distribution of gas phase species n onto material k.

The values of ϕ_{nk} are provided by the FKPM or the radiation transport Monte Carlo module (RTMCM). In general, λ_{njm} depends on $f_{nk}(\varepsilon)$ of the incident gas phase species provided by the plasma chemistry Monte Carlo module (PCMCM). A set of user defined energy dependences can be selected for each type of reaction. In equation (19), two forms of this expression are shown—for chemical sputtering where the reaction has threshold energy ε_t and probability p_0 at reference energy ε_0 with $b = 0.5$, and for low energy enhanced reactions, where ε_M is the upper cutoff energy.

The multi-layer surface site balance model has three categories of species: (1) the base-layer consisting of sites on the solid material in contact with the plasma and whose fractional coverages sum to unity, (2) the over-layer consisting of sites on top of the base surface whose coverages can sum to greater than unity denoting deposition of greater than a monolayer and (3) adsorption sites whose coverage sums to unity. There is a set of rate equations for each class of sites.

θ_k and ζ_k in equation (17) account for this hierarchy of sites. For the base-layer, θ_k limits the interaction of ϕ_{nk} to that fraction of sites not covered by the over-layer. For the over-layer, θ_k limits the interaction of ϕ_{nk} to at most a unity coverage of the over-layer in the event the over-layer is greater than a monolayer thick. ζ_k de-rates the energy (or probability of reaction) of fluxes incident on the over-layer which may penetrate through the over-layer to react with the base-layer. A general expression is used in the SKM to de-rate the ion energy ε:

$$\zeta(\varepsilon, L) = \frac{p(\varepsilon)}{(1+\gamma L)^2}, \tag{20}$$

where L is the thickness of the overlying polymer (in monolayers) and γ is a scaling factor (chosen to be 0.3 for the cases discussed below).

3.4. $f(\varepsilon, \vec{r})$ onto surfaces

The energy distributions of ion, electron and neutral fluxes onto surfaces affect plasma properties through their modification of the surface composition and reactive sticking coefficients. As noted above, the λ_{njm} in the SKM are generally functions of the energy of the incident particles. The PCMCM of the HPEM provides the $f(\varepsilon, \vec{r})$ of neutral and charged particles onto surfaces utilized in the SKM to compute λ_{njm}.

In the HM hierarchy, the FKPM exports source functions for generation of neutrals and ions from all sources (electron impact and heavy particle collisions) to the PCMCM. With these source functions, psuedoparticles are launched from numerical cells throughout the plasma volume. The trajectories of the pseudoparticles are integrated in time using $\vec{E}\vec{B}(\vec{r}, \phi)$, $\vec{E}\vec{B}_S(\vec{r}, \phi)$ from the EMM, MSM and FKPM. The gas phase collisional model is derived from the same reaction mechanism as in the FKPM, which may consume the particles as they traverse the plasma. The distribution of energies of the particles is recorded as a function of the material they strike to produce $f(\varepsilon, \vec{r})$.

The time spent in the PCMCM is difficult to quantify. Pseudoparticles are released from each mesh cell randomly during the rf cycle and their trajectories (and those of their progeny) are followed until they are consumed by a gas phase reaction or strike a surface. So the 'time' spent in the PCMCM is the average transit time of a particle from its birth location to its consumption site or striking a surface. For neutral particles in low pressure plasmas, this could be many milliseconds. Since surface coverages typically evolve slowly compared with nearly every other gas phase process, the phase dependence of $f(\varepsilon, \vec{r})$ onto surfaces is not retained.

3.5. Radiation transport

Radiation transport affects plasma properties in at least two ways. Radiation trapping can lengthen the effective lifetime of excited states, thereby, for example, increasing the likelihood of electron impact multi-step ionization. Radiation incident onto surfaces can initiate, independently or synergistically, surface reactions. In the HM hierarchy, these reactions are included in the SKM. In the HPEM, spectrally resolved fluxes and radiation transport are included in the RTMCM [21].

The RTMCM effectively operates the same as the PCMCM. Sources functions for launching of pseudoparticles representing photons are derived from the densities of excited states produced by the FKPM. The trajectories of the photons are tracked until they are absorbed by a gas phase species or strike a surface. The absorption probability is obtained from a Voigt lineshape function using the natural liftime, collisional broadening and Doppler broadening produced by the gas densities and temperatures. Absorbed photons are re-emitted using a partial-frequency redistribution algorithm. The fluxes and spectra of photons are recorded as a function of material the photons strike, and are exported to the SKM. The rates of photon absorption and re-emission are recorded for each optical transition, and are used to calculate radiation trapping factors which lengthen the natural lifetime of excited states. These factors are exported to the FKPM.

Similar to the PCMCM, the time spent in the RTMCM is difficult to quantify. Pseudoparticles are released from each mesh cell and their trajectories are followed until that quantum of energy is quenched or strikes a surface. So the 'time' spent in the PCMCM is an average of the transit time of a photon from its birth location to its being quenched site or striking a surface. For a heavily trapped transition with a many microseconds lifetime, this time could be tens of microseconds.

3.6. Acceleration

One of the features of plasma equipment modelling is the need to address longer timescales than required for electron kinetics to come into equilibrium. There are long timescale evolution of surface coverages, gas heating and, in the case of complex chemistry, minor species resulting from electron impact dissociation. To achieve a SS, some form of *acceleration* is typically required. Acceleration refers to approximations beyond simply integrating the governing equations in time to more rapidly achieve a SS or HSS.

Time slicing is one form of acceleration. Consider, for example, surface chemistry as represented in the SKM. The time over which the surface coverages come to equilibrium in a typical plasma etching or deposition reactor can be many seconds, whereas the plasma comes into equilibrium with the surface composition in the matter of a few tens of microseconds. Time slicing can achieve effective acceleration by integrating a few microseconds in the FKPM to produce $\vec{\phi}(\vec{r})$ to surfaces with $\alpha(\vec{r})$ and $\beta_{ij}(\vec{r})$ being held constant—followed by many milliseconds of integration in the SKM to update $\alpha(\vec{r})$ and $\beta_{ij}(\vec{r})$ with $\vec{\phi}(\vec{r})$ being held constant. The precise times spent in each module are chosen such that $\vec{\phi}(\vec{r})$, $\alpha(\vec{r})$ and $\beta_{ij}(\vec{r})$ do not significantly change call-to-call. In this manner, the effective acceleration is a factor of hundreds.

When these disparities in timescales between modules cannot be leveraged, or when there is slow time evolution of species within a module, a numerical acceleration technique can be used. In this context, acceleration refers to stopping the simulation, adjusting species densities towards their SS or HSS values and restarting the simulation. A simple acceleration

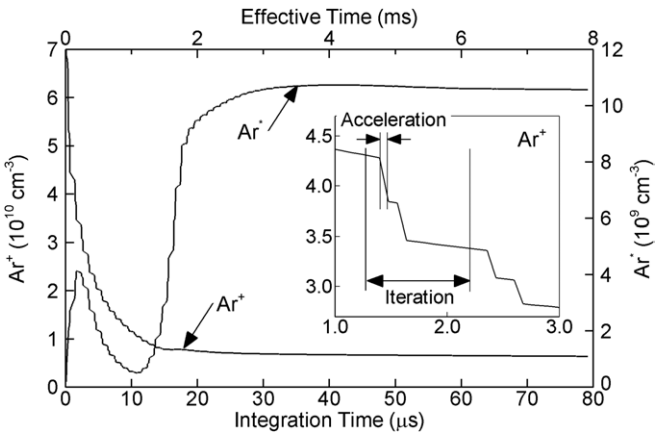

Figure 6. Time evolution of Ar* and Ar+ in an ICP showing acceleration steps during each iteration.

technique is to use the past history of densities to extrapolate the densities into the future:

$$N_{\mathrm{A}}(t_{n+1}) = N(t_n) + f(N_{j<n+1}), \tag{21}$$

where $N_{\mathrm{A}}(t_{n+1})$ is the accelerated density for time t_{n+1}, $N(t_n)$ is the current density and $f(N_{j<n+1})$ is a function of the prior values of N. Since the relative time rate of change of different species may be different, the higher the numerical order of f, the more likely densities of different species will retain their relative values after the acceleration step. The acceleration can be performed on a volume averaged basis or on a point-to-point basis.

A simple acceleration technique used in the HPEM is to linearly accelerate densities with an upper limit and lower limit to prevent over- (or under) acceleration. For example, for acceleration after a period Δt,

$$N_{\mathrm{A}}(t_{n+1}) = N(t_n)(1+\delta), \tag{22}$$

$$\Delta N/\Delta t = (N_n - N_{n-1})/(t_n - t_{n-1}), \tag{23}$$

$$\delta = \xi(\Delta N/\Delta t)(t_n - t_{n-1})/N_n, \tag{24}$$

$$\delta = \min(\delta, \delta_{\max}), \qquad \delta = \max(\delta, \delta_{\min}), \tag{25}$$

where N_{A} is the accelerated value, N_n is the density at time t_n, ξ is an acceleration factor, δ is the fractional change in N due to acceleration, and $\delta_{\min}$ and $\delta_{\max}$ are the lower and upper limits on δ.

An example of acceleration from the HPEM is shown in figure 6 for an ICP sustained in argon. In this particular case, the time spent in the FKPM during any given iteration is 1 μs. Two accelerations per iteration during the FKPM are performed. The time between accelerations, Δt, is 0.2 μs. The last 0.6 μs of integration during the call to the FKPM is performed without acceleration to allow any transients introduced by acceleration to damp out. The stair-step like appearance of the curves indicates the discrete changes in density resulting from acceleration. The timescale on the top axis is at best an approximate accelerated or effective time due to there being upper and lower limits placed on the acceleration.

The time history of these densities indicates too rapid an acceleration (that is, ξ is too large). The Ar* density is initially over-accelerated, resulting in an overshoot of density. The acceleration then decreases the Ar* density to recover from the overshoot before a more temperate acceleration occurs.

Certain quantities should be preserved or rescaled following an acceleration step to prevent unphysical transients. For example, fluxes and energy densities can be scaled with the change in the number densities to keep velocities and temperatures constant. Charge densities, $\rho(\vec{r})$, should be preserved to prevent electric fields from being perturbed due to the acceleration. In the HPEM, $\rho(\vec{r})$ is preserved by adjusting the values of the electron density after acceleration.

Note that with any low order acceleration technique, the integration timescale may lose meaning due to the non-linearity of how species densities actually evolve. This lack of a well-defined timescale may not be particularly important in simulations of SS or HSS conditions. To maintain the integrity of the timescale, acceleration techniques must be of high order.

3.7. Sequencing of modules

A flow chart with the sequence and the approximate time spent in each module of the HPEM is shown in figure 7 for a HSS case of an ICP. The process begins with an estimate of densities which provides conductivities to obtain circuit parameters in the CM and to solve the wave equation in the EMM. $\vec{E}\,\vec{B}(\vec{r},\phi)$ from the EMM are then used in the EETM to obtain $kS_{\mathrm{e}}(\vec{r},\phi)$ for the FKPM. The FKPM exports $kS_{\mathrm{e}}(\vec{r},\phi)$, $kS(\vec{r},\phi)$, $N\phi T(\vec{r})$ and $\vec{E}_{\mathrm{S}}(\vec{r},\phi)$ to the PCMCM and RTMCM which produce fluxes to surfaces for the SKM, which update $\alpha(\vec{r})$ and $\beta_{ij}(\vec{r})$. This then constitutes an *iteration*.

In time-slicing fashion the time spent in each module is not particularly meaningful for a SS or HSS case. The time in a module merely needs to be sufficient to process its input data and produce its output data. For example, nearly 1 s of integration in the SKM is required for the surface coverages to significantly respond to a change in fluxes whereas the PCMCM exhausts all of its particles in a millisecond or less. The time in the EMCS, 10 μs, is somewhat arbitrary and intentionally inflated here. The important scaling parameter to achieve acceptable statistics in the EMCS is the product of the number particles times the number cycles that statistics are binned by phase, Nk. Experience has shown that having a smaller value of N and larger value of k provides the best statistics as this enables the tail of $f(\varepsilon)$ to be better populated.

3.8. Numerical techniques

Since very different algorithms may be used in different modules of a HM, the numerical solution techniques used in those modules may also vary. However, in order to minimize loss of fidelity in transferring data between modules, and to minimize effects such as numerical diffusion, meshes and differentiation techniques should be common to all modules.

In the HPEM, a single common structured, rectilinear mesh is used in all modules. Densities, temperatures, potentials and magnetic fields are solved for at the vertices of the mesh, whereas fluxes and electric fields are solved for at the mid-points between vertices. Material properties (e.g. permittivity, permeability, conductivity) are separately

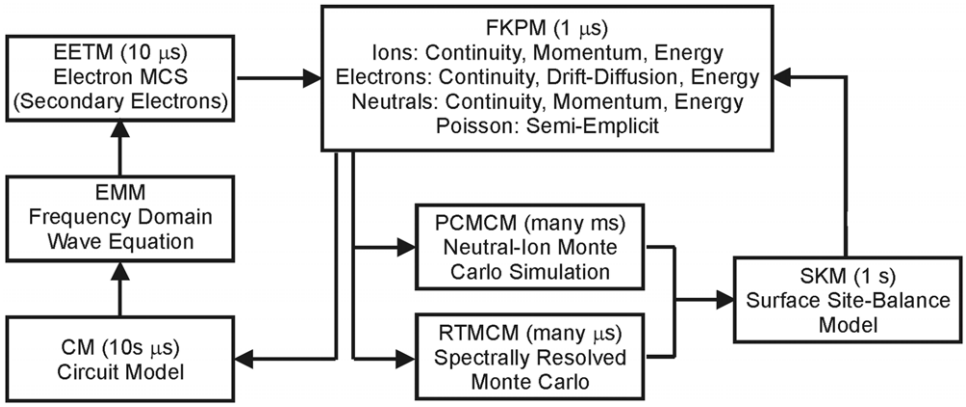

Figure 7. Flow chart of a full case of the HPEM showing order of calling modules and approximate time spent in each module.

specified at the vertices and in the interior of the numerical cells. This allows, for example, for the boundary between a metal and dielectric to be owned by either material.

The solution of Poisson's equation over large dynamic ranges in charge density requires that discretization and construction of divergence terms be fully conservative. This can be accomplished by using finite volume techniques for operators. For example, the time rate of change of a density at mesh point i, N_i, is the negative divergence of the flux at i:

$$\frac{\partial N_i}{\partial t} = -(\nabla \cdot \vec{\phi})_i = \sum_j A_{ij}\phi_{ij}. \tag{26}$$

In finite volume form, the negative divergence is the weighted sum, by A_{ij}, over nearest neighbour mesh points j of the fluxes between i and j, ϕ_{ij}. Although there are mathematical representations of A_{ij}, the physical interpretation is A_{ij} = (area of face of cell i between i and j)/(volume of cell i). To improve stability and increase numerical order, where possible ϕ_{ij} are expressed as upwind or downwind using donor cell techniques. For example, in one dimension the contribution of fluxes to the density in cell i is

$$\frac{\partial N_i}{\partial t} = A_{i-1/2}0.5(\text{abs}(\phi_{i-1/2}) + \phi_{i-1/2}) + A_{i+1/2}0.5(\text{abs}(\phi_{i+1/2}) - \phi_{i+1/2}), \tag{27}$$

where the first term (fluxes from the left) allows contributions from only positive fluxes and the second term (fluxes from the right) allows contributions from only negative fluxes.

As noted above, matrix solution techniques depend on the format of the matrix. Matrices containing elements from only nearest neighbours with A_{ij} shared with the diagonal (e.g. five-point numerical molecule) are typically solved using SOR (successive over relaxation). Matrices containing elements from next-nearest neighbours with A_{ij} which are not shared with the diagonal (e.g. nine-point molecules) are solved using sparse matrix technique such as DSLUCS (BiConjugate gradient squared method with incomplete LU decomposition preconditioning) or DSLUGM (generalized minimum residual method with incomplete LU factorization) [32]. Convergence criteria for electric potential or densities and fluxes contributing to charge densities are $<10^{-7}$.

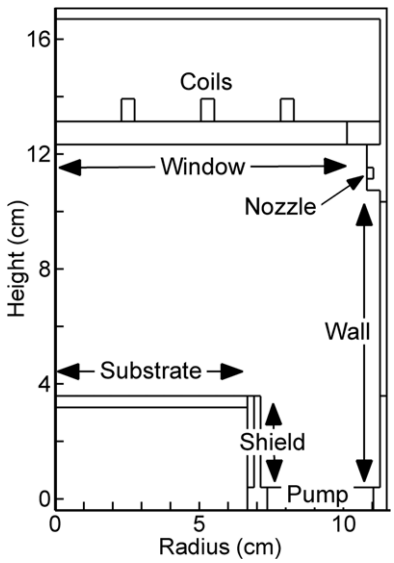

Figure 8. Schematic of the cylindrically symmetric ICP reactor used in the example cases. The surfaces are labelled for later reference for fluxes and surface coverages.

4. Modularity of physics models

One of the features of HM is the ability to use different algorithms to represent the same physics. To demonstrate this modularity a series of cases will be discussed for an ICP where different algorithms are used for electron transport. The ICP is sustained in 10 mTorr of argon using the reactor shown in figure 8. The coils are powered at 10 MHz with currents adjusted by the CM to deliver 300 W. The coils capacitively couple through the insulator to the plasma, a process included in solution of Poisson's equation in the FKPM. The substrate is biased with a constant voltage (amplitude 200 V) at 5 MHz. The modules employed are EMM, EETM, FKPM, SKM and RTMCM.

The differences between the cases will be in the options for addressing electron energy transport—EEE or EMCS. When using the EMCS, several variants are examined—including or excluding electron–electron (e–e) collisions, and using either a collisional or anomalous skin-depth model for penetration of the electromagnetic field into the plasma. The anomalous

skin-depth model is represented by kinetically computing $\vec{j}(\vec{r},\phi)$ in the EMCS for use in the solution of the wave equation in the EMM. e–e collisions are represented by a particle-mesh algorithm wherein electron particles collide with electrons selected from real time recordings of $f(\varepsilon)$ [25].

The density of Ar^+ and T_e are shown in figure 9 for the EEE, EMCS and EMCS with e–e collisions. (For the EMCS cases, $T_e(\vec{r}) = (2/3)\int \varepsilon f(\varepsilon,\vec{r})\varepsilon^{1/2}d\varepsilon$.) In these cases, the solution of the wave equation uses a collision current density (that is, $\vec{j} = \sigma \vec{E}$) and so does not directly address anomalous behaviour. Although non-local transport is included in the EMCS, those currents are not self-consistently fed back to the wave equation. Self-consistent feedback is addressed below. The peak ion density in all cases is in excess of 10^{11} cm^{-3}, producing partial ionizations (when accounting for gas heating of up to 740 K) of 0.1–0.4%. When using the EEE, the peak ion density is 8.6×10^{11} cm^{-3}, as shown in figure 9(*a*), with a T_e having a maximum of 4.7 eV under the coils where $\vec{E}\vec{B}(\vec{r},\phi)$ is largest (the collisional skin depth is 1–2 cm). Due to the high thermal conductivity afforded by the low gas density, T_e decreases by only a few tenths of an electronvolt across the plasma. This produces a nearly uniform rate coefficient for electron impact ionization. With this uniform rate coefficient, the electron impact ionization sources mirror the plasma density which takes on a fundamental mode diffusion profile.

When using the EMCS without e–e collisions the peak ion density decreases to 2.0×10^{11} cm^{-3} with an off-axis peak, as shown in figure 9(*b*). The scalloping of plasma density below the coils results from the oscillating sheath from capacitive coil coupling. T_e is maximum at 3.8 eV under the coils where $\vec{E}\vec{B}(\vec{r},\phi)$ is the largest. T_e also has local maxima in the periphery of the reactor while being minimum on the axis. The maxima in the periphery is partly explained by the rf bias on the substrate and the capacitive coupling from the coils that produces oscillating sheaths and some amount of local heating. The long-mean-free path transport of electrons accelerated in the ICP skin layer can traverse the reactor and reflect from these sheaths. The end result is an electron impact source function which is centred under the coils and so produces an off-axis maximum in Ar^+.

The on axis local minimum in T_e results from a pooling of low energy electrons at the maximum of the time averaged plasma potential at the centre of the reactor. This is more clearly seen in $f(\varepsilon)$ as a function of height appearing in figure 10. $f(\varepsilon)$ at 12 cm in the electromagnetic skin layer and at 4 cm in the presheath produced by the substrate bias are nearly Maxwellian with elevated tails. Those $f(\varepsilon)$ near the centre of the reactor (6, 8, 10 cm) have exaggerated thermal components. This results from low energy electrons that are trapped in the time averaged positive plasma potential in the middle of the reactor. In the absence of e–e collisions, there is insufficient exchange of momentum with more energetic particles for the trapped electrons to escape the potential well and so there is pooling. Since in the SS electron sources must equal electron losses, after a critical amount of pooling the electro-positive potential at the centre of the reactor flattens sufficiently to allow low energy electrons to escape.

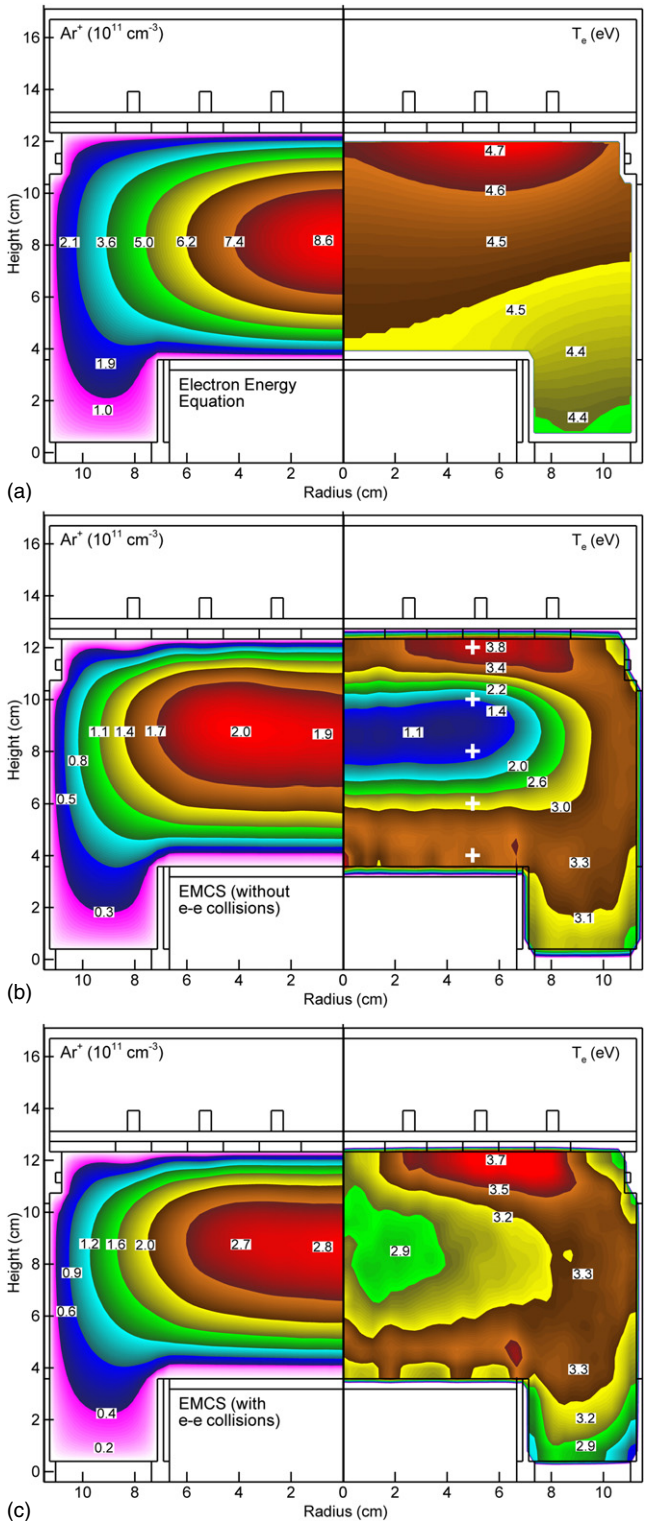

Figure 9. Parameters for an ICP when using different options for electron energy transport. (left) Ar^+ density and (right) electron temperature. (*a*) Electron energy equation, (*b*) EMCS without e–e collisions, (*c*) EMCS with e–e collisions. (The crosses indicate where $f(\varepsilon)$ is shown in figure 10).

When including e–e collisions, the maximum ion density is 2.8×10^{11} cm^{-3} with an extension off axis, as shown in figure 9(*c*). T_e at the centre of the reactor at the maximum of the time averaged plasma potential increases up to 2.9 eV

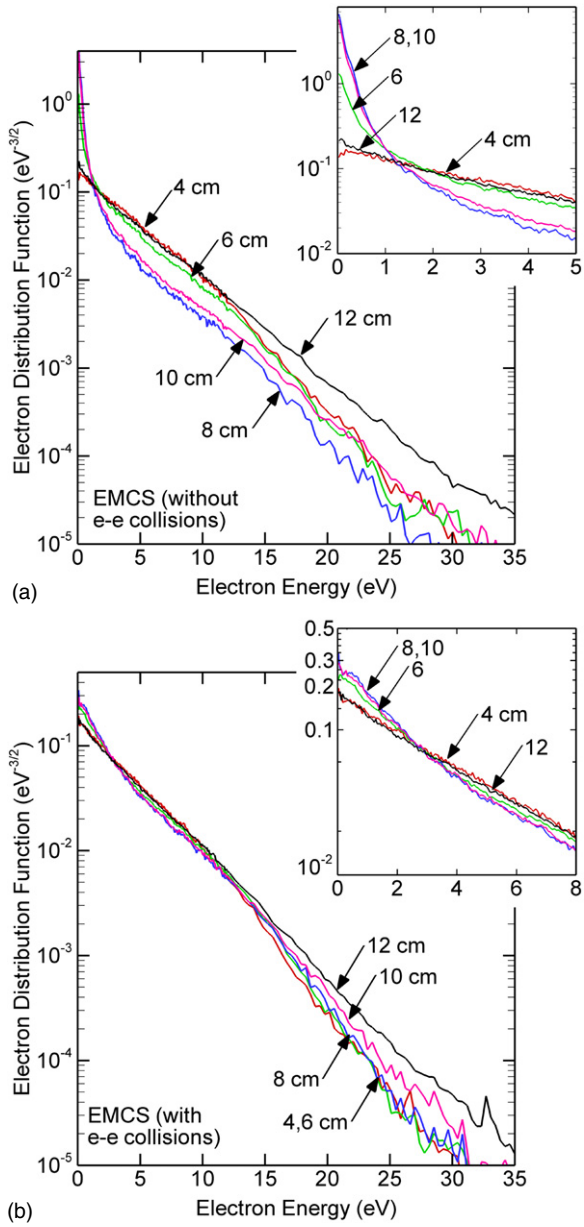

Figure 10. $f(\varepsilon)$ in the Ar ICP as a function of height at a radius of 5 cm for the conditions of and locations shown figure 9. (*a*) EMCS without e–e collisions and (*b*) with e–e collisions.

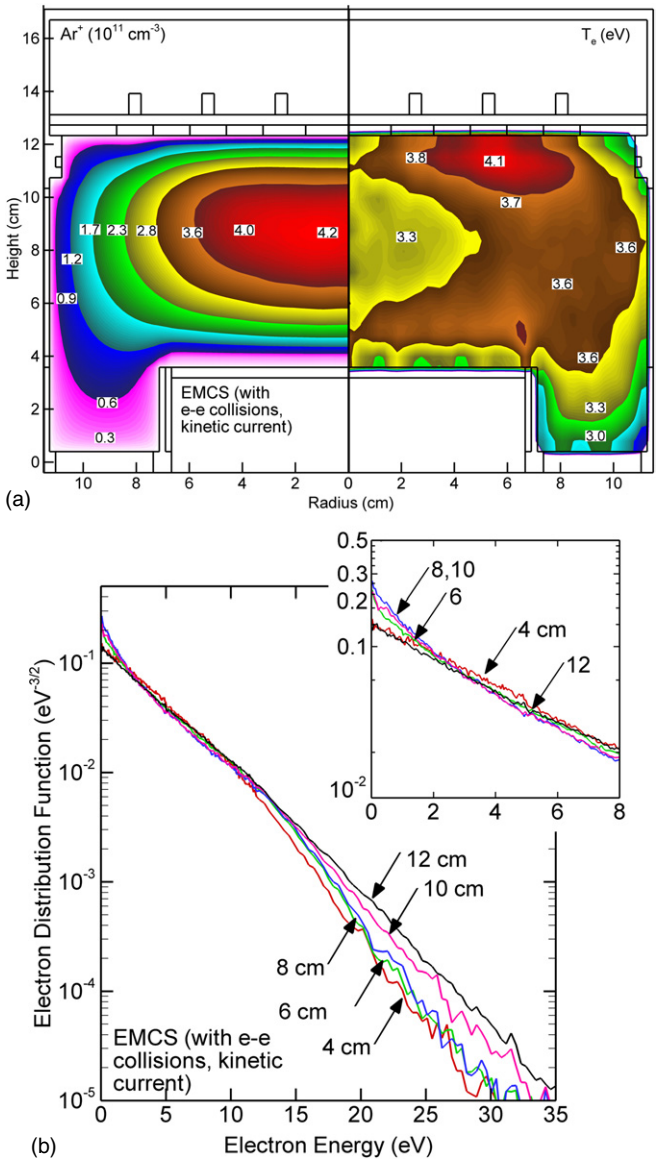

Figure 11. Plasma properties when including kinetically derived electron currents from the EMCS in the EMM. (*a*) Ar^+ density and electron temperature, (*b*) $f(\varepsilon)$ as a function of height at a radius of 5 cm for the conditions of figure 9.

compared with 1.1 eV without e–e collisions. This warming of the electron swarm results from the thermalization of $f(\varepsilon)$ towards a Maxwellian afforded by e–e collisions. As shown in figure 10(*b*), pooling of electrons in the low energy portion of $f(\varepsilon)$ where the Coulomb cross section is large is significantly abated by e–e collisions.

The EMCS, being a kinetic and non-local simulation, captures the anomalous nature of the electromagnetic skin layer. In order to feed that anomalous behaviour back to the EMM, the option exists to kinetically derive plasma electron currents in the EMCS and import those currents into the EMM [26]. Using the modularity afforded by the HPEM, this is accomplished through a function in the EMM that provides the plasma current density. Operationally, this is performed by summing the electron trajectories in the EMCS, binning them by phase in the rf cycle and Fourier analysing the resulting currents to produce a local amplitude and fixed phase factor. Plasma current in the EMM is then

$$\vec{j}(\vec{r},\phi) = \vec{j}_e(\vec{r})\exp(i\phi + \phi_0(\vec{r})) + \sigma_1\vec{E}(\vec{r},\phi), \tag{28}$$

$$j_{EMCS}(\vec{r},\phi_k) = \sum_i q_i v_i(\vec{r})\delta((t_i - t_0)\omega/\Delta\omega), \tag{29}$$

where σ_1 is the conductivity due to ions, $j_e(\vec{r})$ the amplitude of the harmonic electron current having phase offset $\phi_0(\vec{r})$ and $j_{EMCS}(\vec{r},\phi_k)$ is the electron current for phase bin ϕ_k that is Fourier analysed to provide $j_e(\vec{r})$ and $\phi_0(\vec{r})$.

An example of employing this option in the EMM is shown in figure 11 when also using the EMCS with e–e collisions. Compared with the case when using collisional electron currents in the EMM, the ion density increases from

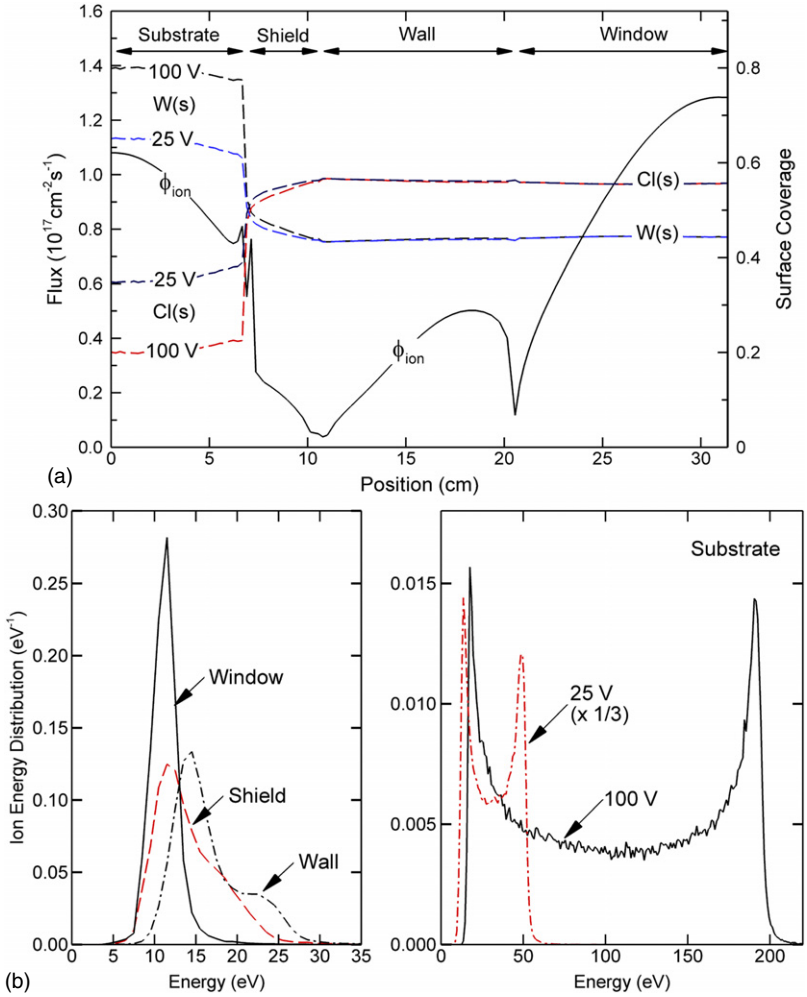

Figure 12. Surface coverages and incident fluxes for an Ar/Cl_2 ICP with an CCP bias on the substrate. (*a*) Coverage of Cl(s) and W(s) and total ion flux as a function of surface position, (*b*) $f(\varepsilon)$ of all ions incident on surfaces as a function of position.

2.8 to 4.2×10^{11} cm^{-3} which is largely attributable to a deeper penetration of the electromagnetic field into the plasma, a more uniform T_e and a raising of the tail of $f(\varepsilon)$.

5. Surface chemistry and boundary conditions

The interaction between modules in a HM hierarchy is well illustrated by the FKPM and SKM of the HPEM. Recall that the purpose of the SKM is to provide surface reaction probabilities for gas phase species incident onto surfaces. The SKM computes coverages of surface species to provide these reaction probabilities. As a first example, we implemented a simple surface reaction mechanism for the adsorption and recombination of Cl atoms in the ICP reactor sustained in an Ar/Cl_2 gas mixture:

$$Cl(g) + W(s) \rightarrow Cl(s) \qquad p = 0.20, \tag{30}$$

$$Cl(g) + Cl(s) \rightarrow Cl_2(g) \qquad p = 0.15, \tag{31}$$

$$Ar^*(g) + Cl(s) \rightarrow Cl(g) + W(s) + Ar(g) \qquad p = 0.20, \tag{32}$$

$$M^+(g) + Cl(s) \rightarrow Cl(g) + W(s) + M(g), \tag{33}$$

where p is the probability for reaction. In this mechanism, gas phase Cl(g) atoms adsorb as Cl(s) on bare wall site W(s). Cl(g) reacts with Cl(s) to desorb as Cl_2(g). Ions M^+(g) can sputter Cl(s) to produce Cl(g) with ε_t =15 eV, ε_0 = 60 eV and p_0 = 1.0 (see equation (19)).

The reaction mechanism was implemented for an Ar/Cl_2 = 90/10, 10 mTorr mixture with an ICP power of 600 W and a fixed bias on the substrate. Typical results are shown in figure 12 for an rf bias of 25 V (dc self-bias = −12.4 V) and 100 V (dc self-bias = −79 V). $f(\varepsilon)$ of ions incident onto the dielectric window has a maximum extent of approximately the floating plasma potential since the window rapidly charges and discharges during the rf cycle, and is essentially a floating body. The grounded shield and walls have $f(\varepsilon)$ extending to higher energies to reflect more significant oscillation of the rf sheath at their boundaries compared with the dielectric window. $f(\varepsilon)$ incident on the substrate shows the full extent of the rf oscillation. The end result is that the Cl(s) coverage on the window and sidewalls is largely determined by an equilibrium between Cl(g) adsorption and Cl(g) recombination. This produces a fractional coverage of Cl(s) of about 0.55 and W(s) of 0.45 for the 100 V bias. The probability for Cl(g) *disappearing* when striking the surface

is 0.17 and for *recombination* (that fraction producing Cl_2(g)) is 0.084. On the substrate where the ion energies exceed the threshold for sputtering Cl(s), its fractional coverage decreases to 0.19 for the 100 V bias, as the majority of the surface sites are bare. The probability for Cl(g) *disappearing* when striking the substrate is 0.19 and for *recombination* is 0.031.

For the 25 V case, the fractional coverages on the non-substrate surfaces do not significantly change from the 100 V case as the ion energies are largely below the desorption threshold. On the substrate, with proportionately lower ion energies than the 100 V case, the desorption probability by ion bombardment is smaller. As a result, the Cl(s) fractional coverage rises to 0.35. The probability for Cl(g) *disappearing* striking the surface is 0.18 and for *recombination* is 0.054.

6. Complex surface chemistry in an HM

Fluorocarbon plasmas are extensively used for the selective etching of inorganic dielectrics such as Si_3N_4, SiO_2 and *low-k* materials [27]. Selectivity between, for example, SiO_2 and Si is obtained through deposition of a fluorocarbon CF_n polymer layer having thickness of a few tenths to many nanometres on materials having ion bombardment of many tens to hundreds of electronvolts. The CF_n provides the F and C atoms to remove the Si and O atoms in SiO_2 producing volatile products such as SiF_n, COF_n and CO_2. Etch rates are slower on, for example, Si since it lacks oxidizing atoms to remove the C in the overlying films. Low energy ion activation enhances the rate of polymer growth, while high energy ions and F atoms consume the layer through sputtering and etching. The polymer layer inhibits the delivery of activation energy to the substrate, where SiO_2 polymer complexes are etched away to volatile SiF_3 and COF_n [28]. This results in an inverse relationship of etch rate to polymer thickness [29].

These fluorocarbon films are deposited by fluxes of neutral CF_n radicals and their ions, and eroded by non-reactive ions. The same processes occur on both wafer and non-wafer surfaces of the reactor. Differences in relative abundances of the radical and ion fluxes, and their energies, determine the polymer thickness on the same materials in different locations. Reactions with the underlying surfaces determine differences in polymer thickness between materials.

The composition of the fluorocarbon film is represented by the mole fractions of the CF_n(s) ($n = 0$–3) components of the polymer. This composition is important with respect to the chemical reactivity of the film with the underlying surface, and in the rate of cleaning of the films from the plasma chamber walls. For example, the rate of polymer growth depends on the number of available open sites for radicals to attach, which in turn depends on the state of fluorination of the CF_n(s) site. Since the composition of the flux of neutral CF_n(g) radicals, the ratio of neutrals to ions and the ion energies vary along surfaces in the chamber, it is reasonable to expect that the composition of the CF_n films will also vary as a function of position in the reactor [30].

Energetic ions additionally affect this composition by defluorination reactions where C–F bonds are broken, thereby liberating F atoms within the film. UV photon fluxes from the plasma also have the potential to defluorinate the film by also breaking the C–F bonds.

The composition of the fluorocarbon polymer film in the ICP sustained in an Ar/C_4F_8 mixture was investigated using the HPEM. The surface reaction mechanism is based on that discussed in [20]. The reaction mechanism was refined by keeping track of the CF_n(s) binding sites in the polymer film. For example,

$$CF_n(g) + P_m \rightarrow P_m\_P_n, \tag{34}$$

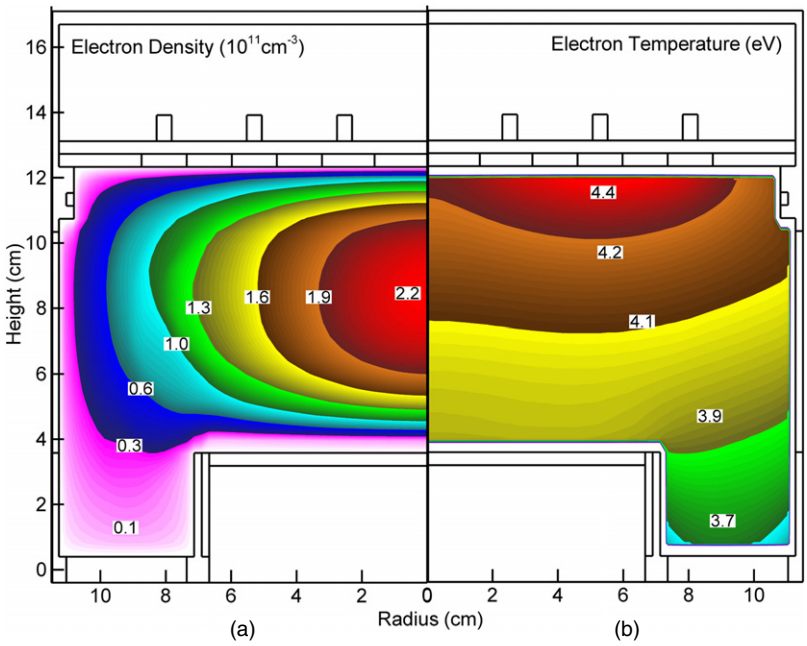

Figure 13. Plasma properties for an Ar/C_4F_8 ICP with a CCP bias on the substrate. (*a*) Electron density and (*b*) electron temperature.

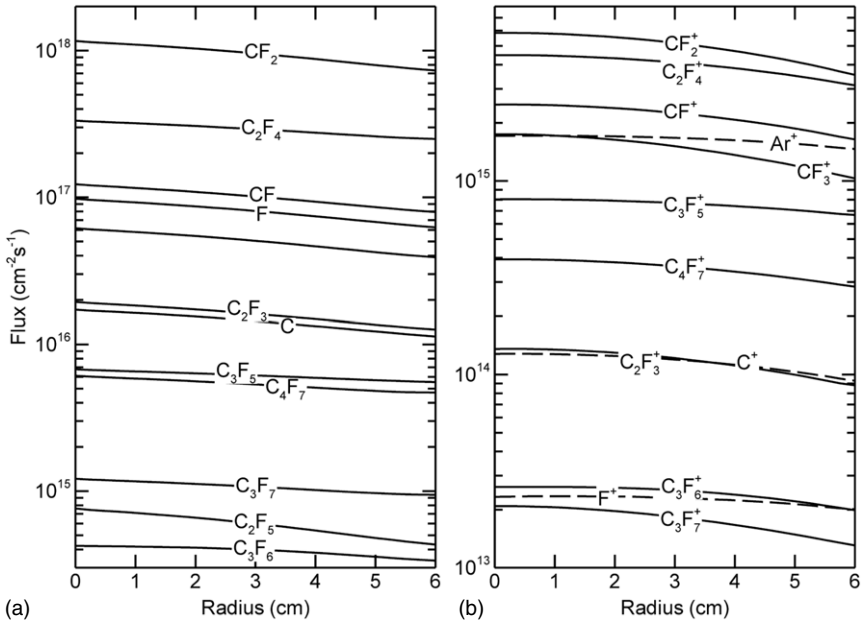

Figure 14. Fluxes to the substrate in the Ar/C_4F_8 ICP reactor: (*a*) neutral fluxes and (*b*) ion fluxes.

where CF_n(g) is an incident gas phase radical and P_m is a carbon atom in the polymer film bonded to m F atoms. A hierarchy of reactions was implemented to account for the C–C bonding and cross-linking of the film. The measure of film composition is the F atom-to-C atom ratio (F/C) in the film. A PTFE-like (polytetrafluoroethylene) film would have $F/C = 2.0$. $F/C > 2$ indicates a film that is F rich; $F/C < 2$ indicates a film that is carbon rich.

The C/F of the film depends on the composition of the incident flux, the relative sticking coefficients of those radicals, their sputtering rates and their rates of defluorination—that is breaking of the C–F bonds in the film and liberation of F atoms. These F atoms are released within the film and so can diffuse both out of the film into the gas phase or to the underlying SiO_2 interface where etching reactions may occur. These defluorination reactions occur through both photon ion bombardment. For example,

$$CF_n(s)+h\nu \rightarrow CF_{n-1}(s) + F(i), \quad (35)$$

$$CF_n(s) + M^+(g) \rightarrow CF_{n-1}(s) + F(i) + M(g), \quad (36)$$

$$F(i) \rightarrow F(g), \quad (37)$$

$$F(i) \rightarrow \text{polymer-}SiO_2 \rightarrow \text{etch products}, \quad (38)$$

where F(i) represents interstitial F atoms.

The HPEM was used to model polymer deposition, its composition and SiO_2 etching in the ICP reactor. The process conditions are Ar/C_4F_8 = 60/40, 10 mTorr, 600 W, 50 sccm with a bias on the substrate from 0 to 250 V at 5 MHz. The Ar/C_4F_8 reaction mechanism is the same as in [31]. The modules used in the HPEM are the EMM, EETM, FKPM, SKM, RTMCM and PCMCM. In the FKPM, ion and neutral momentum and energy equations were solved. The EEE was solved for T_e with the EMCS being used to track the trajectories of secondary electrons. In The RTMCM, resonant radiation from Ar* and F* was tracked.

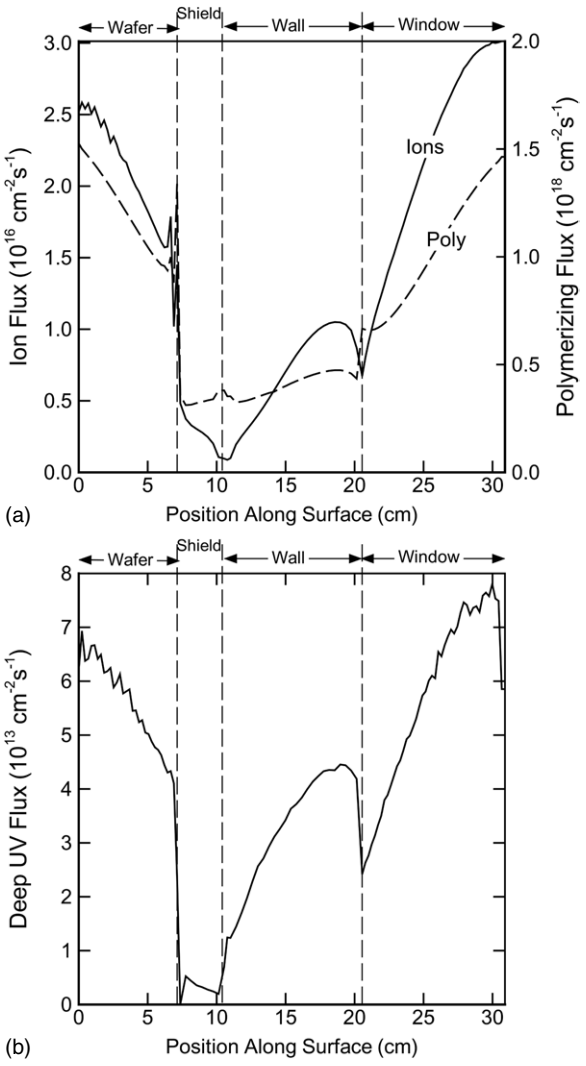

Figure 15. Fluxes to surfaces in the ICP reactor. (*a*) Ion and polymerizing radical fluxes, (*b*) VUV photon fluxes.

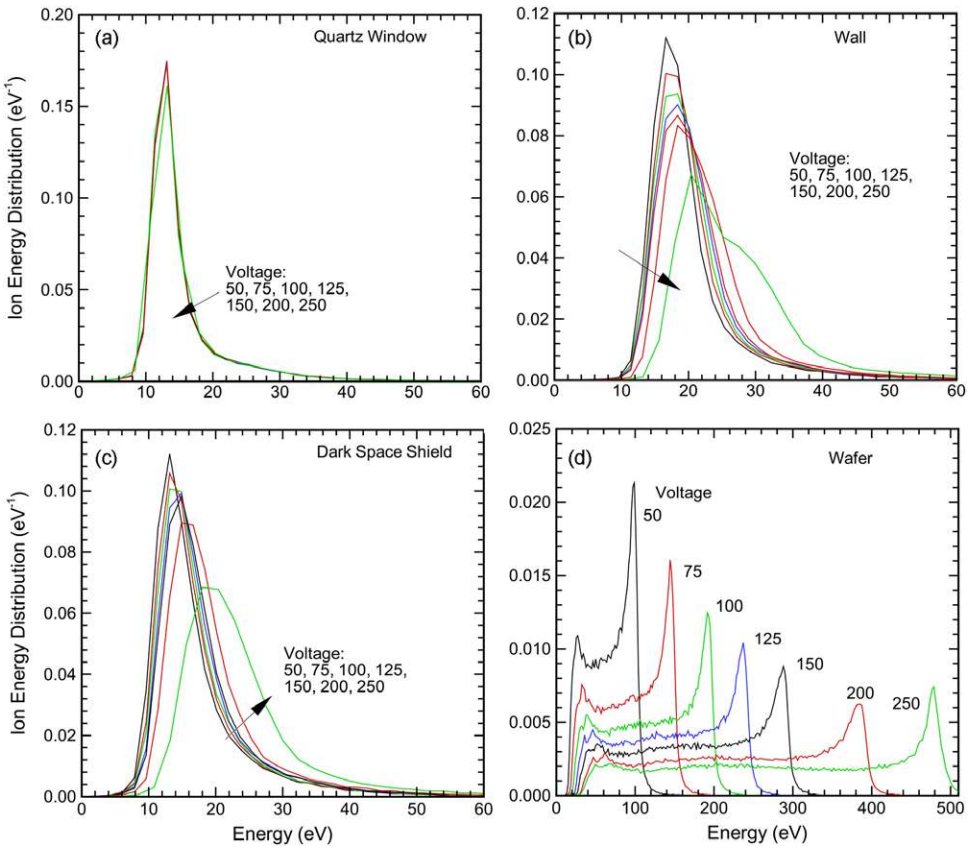

Figure 16. Ion energy distributions to different surfaces in the ICP reactor for substrate biases of 50–250 V.

The electron density and electron temperature for a bias of 200 V are shown in figure 13. The electron density peaks on axis with 2.2×10^{11} cm^{-3}. T_e has a maximum of 4.4 eV under the coils, decreasing to 3.7 eV outside the electromagnetic skin depth. The C_4F_8 is nearly fully dissociated producing fluxes to the wafer that are dominated by CF_n species, as shown in figure 14. With the exception of C_2F_4 (a direct dissociation product of C_4F_8 which is not particularly reactive), the reactive fluxes are primarily composed of CF_2, CF and F.

The fluxes incident on different surfaces are shown in figure 15 and the IEADs are shown in figure 16. Since there is little heating by the CCP bias, the magnitude and relative ratios of fluxes to surfaces change little with bias. The ratio of polymerizing radical fluxes to ion fluxes varies along the surface of the reactor. The ion flux-to-radical flux is largest under the coil where ionization rates are maximum and to the substrate due to ion acceleration. The fluxes of VUV photons largely reflect the line of site from their initial emission to the surface (trapping factors are <5), and so are largest under the coil where production rates are highest.

The IEADs to the window are nearly independent of the bias since the window remains at the floating potential during the majority of the rf cycle. The IEADs to the substrate reflect the full dynamic range of the rf potential including the negative dc bias. The IEADs to the side wall and dark space shield are only weakly dependent on the rf bias since the dc bias reduces the dynamic range of the oscillation of their sheath potentials.

The polymer deposition rates and F/C ratio are shown in figure 17. For biases $\leqslant$50 V, the rates of polymer sputtering are nominal and so the polymer deposition rates as a function of position largely reflect the magnitude of the polymerizing radical flux. For biases $\leqslant$125 V there is net deposition on the substrate. As the bias voltage increases, the rate of sputtering on the substrate increases until 150 V when there is net etching of the SiO_2 substrate. The increase in the deposition rate on the sidewalls and window for high biases is a result of sputtering of CF_n from the substrate and re-deposition on the sidewalls and windows.

The F/C ratio varies from 1.27 to 1.9, indicating that the films are generally carbon rich due in part to defluorination reactions. The highest F/C ratios occur where the ratio of ion-to-radical flux and deposition rates are lowest. At the base of the shield and side walls, the film is PTFE-like. Increasing ion-to-radical fluxes or increasing ion energy promotes defluorination reactions and so decreases the F/C ratio.

7. Sensitivity and accuracy

Hybrid models are no different from other modelling platforms in that the final outcomes are sensitive to the accuracy of the fundamental parameters used in the solutions (e.g. cross sections, surface reaction probabilities) in addition to being sensitive to the accuracy of the algorithms and their solutions. A discussion of the robustness of the databases that might be

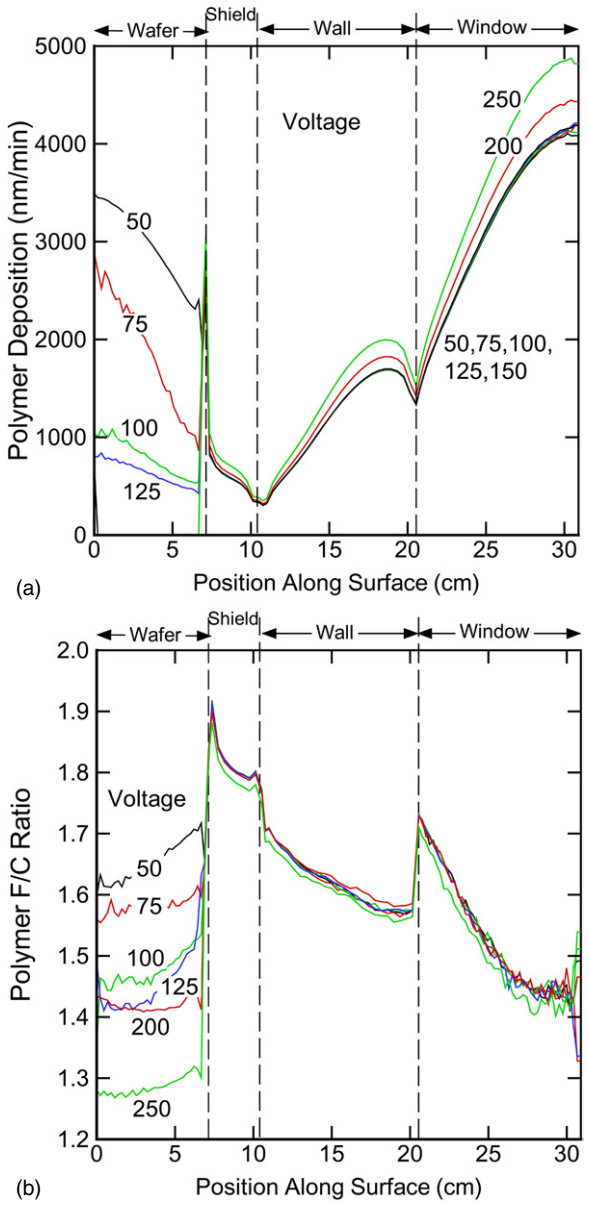

Figure 17. Polymer properties on different surfaces in the ICP reactor for biases of 50–250 V: (*a*) polymer deposition rate, (*b*) F/C ratio.

used in hybrid models is beyond the scope of this review. We will comment on *V&V*—verification and validation.

Verification refers to how accurately the underlying algorithms are numerically solved. Validation refers to how accurately those algorithms reproduce experimental observations. *V&V* is a well established discipline [33]. For example, verification can consist of suites of test problems for which there are analytic solutions against which numerical solutions can be compared. In the case of plasma modelling, the verification suite might include a diffusion dominated positive column discharge sustained in a single gas neglecting excited states and having constant or step function cross sections. Essentially, this is the Schottky theory of the positive column for which there are semi-analytic solutions [34, 35].

HM is highly suited to *V&V* in that algorithms for different physical phenomena in a given module can be exchanged and their solution methods modified without disturbing other modules. For example, the sensitivity of the final solution to whether an electromagnetic skin depth is treated as collisional or anomalous can be isolated independently of the manner of generating source functions. In this sense, HM shares many of the advantages of object oriented programming with respect to *V&V* [36].

8. Concluding remarks

The basis and implementation of HM has been discussed using examples from studies of ICP reactors. HM has demonstrated the ability of addressing a variety of reactor types and physical processes. In addition to implementing advanced physical algorithms as they become available, the future challenges to HM include improving computational techniques to take advantage of multi-core processors and parallel computers. The HM hierarchy is ideally suited to parallel implementation due to the compartmentalization of physics into modules having their own unique timescales.

Acknowledgments

The author thanks his graduate students and post-doctoral research associates who have developed the HM framework in his research group; and the many companies and agencies who have provided support. The author acknowledges the support of the Semiconductor Research Corp. during the authoring of this paper.

References

[1] 2007 *Plasma Science: Advancing Knowledge in the National Interest* National Research Council, Plasma 2010 Committee (National Academy Press) chapter 2
[2] 2003 Modeling and simulation of collisional or near-collisionless low-temperature plasmas (special issue) *Trans. Plasma Sci.* **31** no 4
[3] Rauf S, Gochberg L A, Ventzek P L G and Jack McInerney E 2005 Computer simulation accelerates equipment and process design *Semiconductor International* November 1
[4] Rauf S, Haggag A, Moosa M and Ventzek P L G 2006 *J. Appl. Phys.* **100** 023302
[5] Kim H C, Iza F, Yang S S, Radmilović-Radjenović M and Lee J K 2005 *J. Phys. D: Appl. Phys.* **38** R283
[6] Kolobov V I 2006 Striations in rare gas plasmas *J. Phys. D: Appl. Phys.* **39** R487
[7] Kinder R L and Kushner M J 1999 *J. Vac. Sci. Technol.* A **17** 2421
[8] Vasenkov A V and Kushner M J 2004 *J. Appl. Phys.* **95** 834
[9] Vyas V and Kushner M J 2006 *J. Vac. Sci. Technol.* A **24** 1955
[10] Rauf S and Kushner M J 1997 *J. Appl. Phys.* **82** 2805
[11] Kinder R L and Kushner M J 2001 *J. Vac. Sci. Technol.* A **19** 76
[12] Agarwal A and Kushner M J 2007 *J. Appl. Phys.* **101** 063305
[13] Lu J and Kushner M J 2001 *J. Vac. Sci. Technol.* A **19** 2652
[14] Rauf S and Kushner M J 1998 *IEEE Trans. Semicond. Manuf.* **11** 486
[15] Kinder R L, Ellingboe A R and Kushner M J 2003 *Plasma Sources Sci. Technol.* **12** 561
Kinder R L, Ellingboe A R and Kushner M J 2004 *Plasma Sources Sci. Technol.* **13** 187 (erratum)

[16] Vyas V, Hebner G A and Kushner M J 2002 *J. Appl. Phys.* **92** 6451
[17] Grapperhaus M J and Kushner M J 1997 *J. Appl. Phys.* **81** 569
[18] Grapperhaus M J, Krivokapic Z and Kushner M J 1998 *J. Appl. Phys.* **83** 35
[19] Kushner M J 2003 *J. Appl. Phys.* **94** 1436
[20] Zhang D and Kushner M J 2001 *J. Vac. Sci. Technol.* A **19** 524
[21] Rajaraman K and Kushner M J 2004 *J. Phys. D: Appl. Phys.* **37** 1780
[22] Rauf S and Kushner M J 1998 *J. Appl. Phys.* **83** 5087
[23] Scharfetter D L and Gummel H K 1969 *IEEE Trans. Electron Dev.* **16** 64
[24] Subramonium P and Kushner M J 2002 *J. Vac. Sci. Technol.* A **20** 313
[25] Weng Y and Kushner M J 1990 *Phys. Rev.* A **42** 6192
[26] Vasenkov A V and Kushner M J 2002 *Phys. Rev.* E **66** 066411
[27] Standaert T E F M, Matsuo P J, Allen S D, Oehrlein G S and Dalton T J 1999 *J. Vac. Sci. Technol.* A **17** 741
[28] Matsui M, Tatsumi T and Sekine M 2001 *J. Vac. Sci. Technol.* A **19** 2089
[29] Rueger N R, Beulens J J, Schaepkens M, Doemling M F, Mirza J M, Standaert T E F M and Oehrlein G S 1997 *J. Vac. Sci. Technol.* A **15** 1881
[30] Standaert T E F M, Hedlund C, Joseph E A, Oehrlein G S and Dalton T J 2004 *J. Vac. Sci. Technol.* A **22** 53
[31] Vasenkov A V, Li X, Oehrlein G S and Kushner M J 2004 *J. Vac. Sci. Technol.* A **22** 511
[32] 1993 *SLATEC Common Mathematical Library* Version 4.1, July http://www.netlib.org/slatec
[33] Roache P J 1998 *Verification and Validation in Computational Science and Engineering* (Albuquerque, NM: Hermosa Publishers)
[34] Schottky W 1924 *Phys. Z.* **25** 635
[35] Ecker G 1964 *Proc. Phys. Soc.* B **67** 485
[36] Brok W J M, van Dijk J, Bowden M D, van derMullen J J A M and Kroesen G M W 2003 *J. Phys. D: Appl. Phys.* **36** 1967